In the Name of Allah, The Most beneficiary,
The Most Gracious, The Most Merciful

Dual Solutions for MHD Slip Flow of Nanofluid in the presence of Nonlinear Radiation.

By

Abdul Hafeez.

Department of Mathematics
Quaid-i-Azam University
Islamabad, Pakistan
2017

Dual Solutions for MHD Slip Flow of Nanofluid in the presence of Nonlinear Radiation.

By

Abdul Hafeez

Supervised By

Prof. Dr. Masood Khan.

Department of Mathematics
Quaid-i-Azam University
Islamabad, Pakistan
2017

Dual Solutions for MHD Slip Flow of Nanofluid in the presence of Nonlinear Radiation.

By

Abdul Hafeez

A DISSERTATION SUBMITTED IN THE PARTIAL FULFILLMENT OF THE REQUIREMENT FOR THE DEGREE OF

MASTER OF PHILOSOPHY

IN

MATHEMATICS

Supervised By

Prof. Dr. Masood Khan.

Department of Mathematics
Quaid-i-Azam University
Islamabad, Pakistan
2017

Acknowledgments

In the name of ALLAh, the most Beneficent, Who enabled me to complete my dissertation. I offer my humble gratitude to Holy Prophet MUHAMMAD (peace Be Upon Him), who is forever a touch of guidance and knowledge for humanity as a whole.

I feel highly privileged to express my heartfelt gratitude to my supervisor, Prof. Dr. Masood Khan for his skilful guidance, helpful suggestions and inspiring attitude during the research. His kindness and generous response to my difficulties during the research work to complete the dissertation in time will never forgotten.

I am also thankful to all the teaching staff of our department. Their inspiration and suggestions helped me to complete my research work.

I would like to extend my sincere gratitude to my friends, Hashim Ali Khan, Masood ur Rehman, Shafiq Ahmad and Noor who have supported me and given me confidence to complete this task.

At the end, my appreciation is also expressed to my parents, brothers and other family members for their constant support, love, guidance and encouragement throughout my career.

Abdul Hafeez

July 2017.

Preface

In modern research era, convectional heat transfer fluids like water, kerosene, engine oil and acetone assume a crucial part in numerous industrial segments including power generation, manufacturing and transportation, chemical production, air-conditioning and microelectronics. On the other hand, because of their low thermal conductivity they have restricted heat transfer capabilities. Recently, scientists are curious to develop different methods to increase their heat transfer performance. One of such methods to overcome this limitation is to improve thermal conductivity of conventional fluids via suspensions of nanoparticles in base fluids and led to generate a new composite called "nanofluids". Moreover, this field is much efficient in terms of heat transfer performance. Technically, these suspensions contain the base fluids and the nanoparticles with a size of 1-100 nm which are suspended in them. Current works on nanotechnology has proved that nanoparticles with diameter less than 50 nm that can change properties of the fluid since thermal conductivity of nanoparticles particles was higher than convectional fluids and these are widely used as heat transfer fluids in thermal processes. The common nanoparticles being used are aluminum, copper, iron and titanium or their oxides. Initially, this idea was given by Choi and Eastman [1] where in they concluded that these nanofluids have better conductivity and convective heat transfer coefficient relative to base fluids. Based on their shape, size, and thermal properties, the thermal conductivity can be enhanced by about 40% with low concentration (1-5% by volume) of solid nanoparticles in the mixture. A broad spectrum of their application includes the sterilization of medical suspensions, cooling of heat sinks, hybrid-powered engines and nuclear reactor coolant etc.

The flow and heat transfer phenomena for nanofluids have been a topic of much research over the past two decades. In recent years, numerous analysis have assessed the properties and impact of nanofluids on the heat transfer change in thermal systems. After the work of Choi and Eastman [1], numerous endeavors in this field have been accomplished to formulate the heat and transfer characteristics of nanofluid flows. In 2006, Buongiorno [2] presented a comprehensive study concerning the heat transport in nanofluids and in his work he found an extraordinary rise in the thermal conductivity of nanofluids. After that, Khan and Pop [3] have broken down the boundary layer flow of a nanofluid over a stretching surface. This was probably the first attempt to ponder the flow of nanofluids over stretching sheet by utilizing a model in which the Brownian motion and thermophoresis impacts were considered. A

theoretical analysis has been done by Makinde and Aziz [4] to investigate the impact of convective heat transfer on the flow of nanoparticle past a stretching sheet. Nadeem and Haq [5] extended the work of Khan and Pop [3] by taking the effects of thermal radiation and convective boundary conditions for flow of nanofluids. Mixed convection flow of Casson nanofluids past a stretching cylinder including the magnetic field and temperature dependent thermal conductivity has been examined by Hayat et al. [6] . Furthermore, Hashim and Khan [7] numerically investigated the heat and mass transfer analysis in the flow of Carreau nanofluids. In this article, they utilized the revised model for nanofluids and solutions are obtained with the help of Runge-Kutta numerical technique. A steady three-dimensional flow of Burgers nanofluid over a bidirectional stretching surface is deliberated by Khan et al. [8]. They implemented the convective boundary and nanoparticles mass flux conditions in this analysis. Very recently, Sandeep [9] scrutinized the flow and heat transfer properties of liquid film flow of magnetic-nanofluids. He assumed the variable directional magnetic field with non-uniform heat source/sink for the graphene nanoparticles. Recently several papers concerning nanofluids transport have appeared $[10-12]$.

In recent times, heat transfer problem with the impact of non-linear thermal radiation is one of the thrust fields of contemporary research by reason of their tremendous applications in the field of engineering and physics, like in space technology, including comical flight aerodynamics rocket, in high-temperature processes such as plasma physics and space craft reentry aerodynamics and furthermore it assumes a key part to enhance the heat transfer properties in polymer processing industry. Moreover, the flow problems involving heat transfer process in the presence of non-linear radiation are extremely vital in manufacturing applications, for instance, in design of reliable equipment, gas turbines, nuclear power plants and several propulsion devices for aircraft, missiles, satellites and space vehicles. There are right now some delightful works on the fluid flows with non-linear radiation. Impact of thermal radiation on mixed convection flow over a vertical surface in a porous medium was studied by Bakier [13]. He employ the fourth-order Runge–Kutta method to obtain the numerical solutions of the governing equations. Cortell [14] presented an endeavours to study the flow of viscous fluid over a nonlinear stretched surface by encountering the effects of thermal radiation in the energy equation. Later on, Akbar et al. [15] performed a numerical computation to discuss the MHD stagnation-point flow of nanofluid towards a stretching cylinder. The heat transfer process is analyzed by considering both the thermal radiation and

convective boundary conditions. The MHD flow of nanofluids between two rotating plates in the presence of thermal radiation is examined by Sheikholeslami et al. [16]. In this work, they found that Nusselt number and radiation parameter has direct relationship with each other. Recently, Khan et al. [17] interrogated the heat transfer analysis in a non-Newtonian Carreau fluid flow by encountering the non-linear thermal radiation. In their study, they utilized the non-linear Rosseland approximation for thermal radiation and noticed that the local Nusselt number was reduced for the larger values of magnetic parameter.

With the deepening of the studies, researchers started to find that boundary slip condition portraying the relative motion between the solid surface and the fluid adjacent to the solid surface is an imperative interfacial properties to affect the fluid flow characteristics. There is a finite velocity of the fluid-solid interface and such type of boundary condition for velocity is the so-called boundary slip, and it can be characterized by slip length. Possibly, Navier [18] was the first who proposed the velocity slip boundary condition in which the tangential slip velocity u_w is linearly related to the wall shear stress τ_w, in the form $u_w = L\tau_w$, where L is the slip coeefficient varies with temperature, pressure, normal stress, molecular parameter, and the characteristic of the fluid solid interface. It may be pointed out that there are several physical situations for which slip on a solid surface occurs. For instance, it happens in flow of rarefied gas [19], in flow over lubricated or coated surfaces (Teflon), rough or striated surfaces [20] and most recently, superhydrophobic nano-surfaces [21]. Further, no-slip phenomenon arises in various industrial processes at the boundary of pipes, walls, and curved surfaces. The fluids displaying boundary slip find attention in technological problems like polishing of artificial heart valves and internal cavities. For this reason, researchers and scientists have given considerable attention to incorporate the slip condition at wall rather than no slip condition. For example, one of the earlier study that took into account the slip boundary condition for the boundary layer flow over stretching surface was conducted by Wang [22]. He obtained the numerical solutions for the governing problem by employing Runge-Kutta technique. Hayat et al. [23] explored the heat transfer attributes for the flow of a second grade fluid past a stretching sheet by incorporating the slip effects. In this study, analytical solutions for the momentum and energy equations have been computed via homotopy analysis method. Afterward, Mukhopadhyay [24] made an attempt to consider the partial slip on boundary layer flow of an incompressible viscous fluid with suction and injection. Nadeem et al. [25] looked into the combined effects of partial slip and magnetic

field for the flow of Casson rheological model past a stretching surface. They tackle the non-linear governing ordinary differential equations numerically by utilizing mid-point integration scheme together with Richardson's extrapolation technique. Freshly, Khan and Hashim [26] imparted an article to study the effects of velocity, temperature and solutal slip on the heat and mass transfer analysis of Carreau rheological model. In this analysis, they assumed the flow to be generated by a stretching wedge and achieved the numerical solutions for governing problem. In the view of literature cited above, the presesnt dissertation is arranged as follows:

Chapter one aimes to present some basics definitions, laws and concepts which are used in fluid mechanics and are helpful to understanding the second and third chapters.

Chapter two deals with the dual solution of MHD boundary layer flow and heat transfer of a nanofluid with viscous dissipation by a stretching/shrinking sheet. The obtained differential equations with boundary conditions are solved numerically using bvp4c technique in Matlab. In fact, this chapter is a detailed review of the work done by Dhanai et al. [27] .

Chapter three aims to analyze multiple solutions of a slip flow and heat transfer performance of nanofluid from a permeable shrinking surface with thermal radiation. A transverse magnetic field is applied to examine the effects of MHD on the flow perpendicular to the wall. The dimensionless partial differential equations solved numerically using the same technique as used in chapter two. The influence of the different involved parameters on the velocity, temperature and concentration profiles are discussed through several graphs.

Contents

Chapter 1

Basic definitions, concepts and laws

This chapter contains some fundamental definitions, laws and concepts which are helpful to understanding the first and second chapters.

1.1 Fluid

A fluid is a substance that deforms continuously when shear force is applied. Examples are gases and liquids.

1.1.1 Liquid

A fluid that has a definite volume but no definite shape. Blood, oil and water etc. are examples of liquids.

1.1.2 Gas

It is type of fluid that has no definite shape and volume. Examples are oxygen and nitrogen.

1.2 Fluid mechanics

It tells us the behaviour of a fluid that at rest or in motion. It has two branches:

1.2.1 Fluid statics

Fluid statics describes the properties of fluids at rest.

1.2.2 Fluid dynamics

Fluid dynamics deals the fluid characteristics in state of motion.

1.3 Stress

Stress is a surface force applied on the unit area to the material. In SI, the unit of stress is kg/ms^2 or $Nm^{-2}$and $[M/Lt^2]$ is its dimension. It has two types.

1.3.1 Shear stress

A force acts parallel to the unit area of the infinitesimal surface element, then stress is named as shear stress.

1.3.2 Normal stress

When a force acts normal to the unit area of the infinitesimal surface element, then stress in known as normal stress.

1.4 Strain

When forces are applied externally to the object and its relative change in shape or size is known as strain.

1.5 Viscosity

Viscosity tells us the measurement of fluid's resistance against the flow. Fluids have a low viscosity like as, water called thin, while have a high viscosity like as, honey called thick. There are two types of viscosity.

1.5.1 Absolute (dynamic) viscosity (μ)

Absolute (dynamic) viscosity is the measurement of internal resistance of a fluid against any deformation when a force is acted upon it. Mathematically, it can be denoted as follow

$$\text{absolute viscosity } (\mu) = \frac{\text{shear stress}}{\text{velocity gradient}}. \tag{1.1}$$

The SI unit is Ns/m^2 and $\left[\frac{M}{LT}\right]$ is its dimension.

1.5.2 Kinematic viscosity (ν)

It describes the ratio between dynamic viscosity to the density of fluid. Mathematically, it can be represented as

$$\nu = \frac{\mu}{\rho}. \tag{1.2}$$

The SI unit is m^2/s and $\left[\frac{L^2}{T}\right]$ is its dimension.

1.6 Newton's law of viscosity

It is defined as the shear force which deforms the element of fluid is linearly and directly proportional to the velocity gradient. Mathematically it is followed as

$$\tau_{yx} \propto \frac{du}{dy}, \tag{1.3}$$

this implies that

$$\tau_{yx} = \mu \left(\frac{du}{dy}\right), \tag{1.4}$$

in which τ_{yx} represents the shear force applied on the element of fluid and μ denotes the proportionality constant.

1.6.1 Newtonian fluids

Those fluids which are satisfied the Newton's law of viscosity is named as Newtonian fluid and the value of μ is being constant. Here the shear force (τ_{yx}) is linearly proportional to the

velocity gradient (du/dy). Examples are water and air etc.

1.6.2 Non-Newtonian fluids

The fluids for which there properties are different in any way from the Newtonian fluids are said to be non-Newtonian fluids. Blood, toothpaste and ketchup are the common examples of non-Newtonian fluid. Mathematically, it can be expressed as

$$\boldsymbol{\tau}_{yx} \propto \left(\frac{du}{dy}\right)^{n}, \; n \neq 1, \tag{1.5}$$

this implies that

$$\boldsymbol{\tau}_{yx} = \eta \frac{du}{dy}, \text{ where } \eta = k\left(\frac{du}{dy}\right)^{n-1}. \tag{1.6}$$

In above equation η, k and n are respectively the apparent viscosity, consistency index and index of flow behaviour. For $n = 1$, Eq. (1.6) reduces to Newton's law of viscosity. Stress tensor for the viscous fluid's is followed as

$$\boldsymbol{\tau} = -p\mathbf{I} + \boldsymbol{\mu}\mathbf{A}_1, \tag{1.7}$$

where $\mathbf{A}_1$ indicates for the first Rivlin-Ericksen tensor, that is

$$\mathbf{A}_1 = (\text{grad}\mathbf{V}) + (\text{grad}\mathbf{V})^{\breve{\mathbf{T}}}. \tag{1.8}$$

Using Cartesian coordinates we have

$$\text{grad}\mathbf{V} = \begin{bmatrix} \frac{\partial u}{\partial x} & \frac{\partial u}{\partial y} & \frac{\partial u}{\partial z} \\ \frac{\partial v}{\partial x} & \frac{\partial v}{\partial y} & \frac{\partial v}{\partial z} \\ \frac{\partial w}{\partial x} & \frac{\partial w}{\partial y} & \frac{\partial w}{\partial z} \end{bmatrix}, \; (\text{grad}\mathbf{V})^{\breve{\mathbf{T}}} = \begin{bmatrix} \frac{\partial u}{\partial x} & \frac{\partial v}{\partial x} & \frac{\partial w}{\partial x} \\ \frac{\partial u}{\partial y} & \frac{\partial v}{\partial y} & \frac{\partial w}{\partial y} \\ \frac{\partial u}{\partial z} & \frac{\partial v}{\partial z} & \frac{\partial w}{\partial z} \end{bmatrix}. \tag{1.9}$$

1.7 Stagnation point

A point where the fluid velocity is zero in a flow field is known as stagnation point. It exists in a flow field at the surface of the objects, where the fluid brings to the rest at the object.

1.8 Porous medium

Porous medium is referred to as, a material which contain pores. In nature these pores are irregular, and the fluid flows through these pores. Wood, cements, soil etc. are the common examples of porous medium.

1.9 MHD (Magnetohydrodynamics)

MHD (Magnetohydrodynaimics) is the study which deals with the mutual interaction of magnetic field and fluid flow.

1.10 Nanofluid

A nanometer-sized particles $(1 - 100$ nm) that contains in a fluid is named as nanofluid. It brought about a colloidal interference of nanoparticles in a base fluid. Usually it is made of carbides, oxides, carbon nanotubes or metal. Choi [1] was the first who presented nanofluid in 1995.

1.11 Skin friction coefficient

Certain amount of drag appears when fluid is passing through a surface is named as skin friction coefficient, and occurs between the fluid and the solid surface which causes to slow the fluid's motion. It can be define as follow

$$C_f = \frac{\tau_w}{\frac{1}{2}\rho U_w^2}, \tag{1.10}$$

whereas τ_w names for wall shear stress, ρ the fluid density and U_w indicates the velocity.

1.12 Dimensionless numbers

1.12.1 Nusselt number

It is a dimensionless quantity. In heat transfer at a surface with in a fluid, Nusselt number represents the convective to conductive heat transfer ratio. Mathematically

$$Nu_L = \frac{h\Delta T}{k\Delta T/L} = \frac{hL}{k}, \tag{1.11}$$

in which h represents convective heat transfer, L names for characteristic length and k stands for thermal conductivity.

1.12.2 Reynolds number

The ratio of inertial to the friction forces describes the Reynolds number. It is a dimensionless number, and is used to recognize the flow behaviours like laminar or turbulent flow. Mathematically, it can be written as

$$\mathrm{Re} = \frac{\rho v^2/L}{\mu v/L^2} = \frac{uL}{\nu}. \tag{1.12}$$

Here u represents the fluid velocity, L denotes the characteristic length and ν is the kinematic viscosity. Reynolds number is used to describe the different kinds of flow depends the value of Reynolds number. When $\mathrm{Re} < 2300$ the flow is laminar and when $\mathrm{Re} > 4000$ the flow is turbulent. Also the flow is transient if $2300 < \mathrm{Re} < 4000$.

1.12.3 Prandtl number

The ratio of momentum diffusivity (ν) to thermal diffusivity is named as Prandtl number. Mathematically

$$\mathrm{Pr} = \frac{\nu}{\alpha} = \frac{\mu/\rho}{k/\rho c_p} = \frac{\mu c_p}{k}, \tag{1.13}$$

where μ denotes the dynamic viscosity, c_p stands for specific heat and k represents the thermal conductivity. For small Prandtl number $(\mathrm{Pr} < 1)$, it shows that the thermal diffusivity dominates, while for large Prandtl number $(\mathrm{Pr} > 1)$, the momentum diffusivity dominates the behaviour. Also in heat transfer, it can be used to control the thermal and momentum boundary

layer thickness.

1.12.4 Hartmann number

Electromagnetic to viscous forces ratio is termed as Hartmann number. Mathematically Hartmann number can be denoted as

$$Ha^2 = \frac{\sigma B_0^2 L}{U\rho}, \tag{1.14}$$

Here σ denotes the electrical conductivity, B_0 the applied magnetic field, L the characteristic length, U indicates the velocity and ρ stands for density of fluid.

1.13 Some basic laws

1.13.1 Law of mass conservation

In any isolated system the total mass will remain constant is referred as law of mass conservation. It means that mass can neither be destroyed or created, however in space, it may be rearranged. Mathematically it can be expressed as

$$\frac{d\rho}{dt} + \rho\boldsymbol{\nabla}.\mathbf{V} = 0, \tag{1.15}$$

or

$$\frac{\partial\rho}{\partial t} + (\mathbf{V}.\boldsymbol{\nabla})\,\rho + \rho\boldsymbol{\nabla}.\mathbf{V} = 0, \tag{1.16}$$

or

$$\frac{\partial\rho}{\partial t} + \boldsymbol{\nabla}.\,(\rho\mathbf{V}) = 0. \tag{1.17}$$

It is referred as continuity equation. For the steady flow the continuity equation becomes

$$\boldsymbol{\nabla}.\,(\rho\mathbf{V}) = 0, \tag{1.18}$$

and for the steady and incompressible fluid, the continuity equation be made as

$$\boldsymbol{\nabla}.\mathbf{V} = 0. \tag{1.19}$$

1.13.2 Law of momentum conservation

In any closed system the total amount of momentum is remains constant is known as law of momentum conservation. Generally it is followed by

$$\rho\frac{d\mathbf{V}}{dt} = \text{div}\,\boldsymbol{\tau}+\rho\mathbf{b}, \tag{1.20}$$

in which $\boldsymbol{\tau}$ represents the Cauchy stress tensor and $\mathbf{b}$ refers for body force.

1.13.3 Law of energy conservation

In an isolated system the total amount of energy is remains constant is named as law of energy conservation. It can neither be destroyed nor created, although it transforms one to another form. Generally

$$\rho\left(\frac{d\mathbf{e}}{dt}\right) = -\boldsymbol{\nabla}.\mathbf{q}+\rho r + \boldsymbol{\tau}.\mathbf{L}. \tag{1.21}$$

Here $\mathbf{e}$ stands for specific internal energy, $\mathbf{q}$ indicates heat flux vector and r refers for thermal radiation.

Without thermal radiation, energy equation becomes

$$\rho c_p\frac{dT}{dt} = \boldsymbol{\tau}.\mathbf{L}+k\boldsymbol{\nabla}^2T. \tag{1.22}$$

Here $\mathbf{e} = c_pT$, $\mathbf{q} = -k\boldsymbol{\nabla}T$, k stands for thermal conductivity and T for temperature. Here $\boldsymbol{\tau}.\mathbf{L}$ refers for viscous dissipation.

1.13.4 Law of concentration

For nanofluid, mathematically the concentration equation is of the form

$$\frac{\partial C}{\partial t} + \mathbf{V}.\nabla C = \nabla\left(D_B\nabla C + \frac{D_T}{T_\infty}\nabla T\right). \tag{1.23}$$

Here C refers the nanoparticle concentration, T indicates the mean temperature, D_T the coefficient of diffusibility and D_B names the Brownian motion parameter.

1.14 Ohm's law

The current density ($\mathbf{J}$) mathematically can be known as

$$\mathbf{J} = \sigma \left(\mathbf{V} \times \mathbf{B} + \mathbf{E} \right), \tag{1.24}$$

where σ is the electrical conductivity of the fluid.

When electric field $\mathbf{E}$ =0, it becomes

$$\mathbf{J} = \sigma \left(\mathbf{V} \times \mathbf{B} \right). \tag{1.25}$$

Now the Lorentz force becomes

$$\mathbf{J} \times \mathbf{B} = \sigma \left(\mathbf{V} \times \mathbf{B} \right) \times \mathbf{B}, \tag{1.26}$$

where

$$\mathbf{B} = \left(0, B_0, 0 \right), \tag{1.27}$$

which implies that

$$\mathbf{J} \times \mathbf{B} = - \sigma B_0^2 \mathbf{V}. \tag{1.28}$$

For velocity field ($\mathbf{V} = \left(u\left(x, y\right), v\left(x, y\right), 0 \right)$), the Lorentz force becomes

$$\mathbf{J} \times \mathbf{B} = - \sigma B_0^2 u \hat{\imath}. \tag{1.29}$$

Chapter 2

MHD boundary layer flow and heat transfer of nanofluid with viscous dissipation by a stretching/shrinking sheet: Dual solution

2.1 Introduction

This chapter presents a numerical study of magneto-hydrodynamics (MHD) boundary layer flow of a nanofluid past a permeable stretching/shrinking sheet using bvp4c technique. The effect of viscous dissipation is taken into account. The governing equations of the problem based on boundary layer approximation are transformed into a non-dimensional form by introducing the local similarity variables. The flow is therefore governed by a mass transfer parameter, Lewis number, Prandtl number, Eckert number, thermophoresis and Brownian motion parameters. This study presents the dual solution for the skin friction, Nusselt number and nanoparticle volume friction for various pertinent parameters in some domain with critical values ($s_c \leq s$) and ($A_c \leq A$). Also in the Nusselt number the existence domain is found to have two unique solutions with stretching/shrinking parameter A and power law parameter β. This study shows that the skin friction reduces with increasing the power law parameter β and decreases with an

increase in magnetic field. This chapter presents a detailed survey of a paper by Dhanai et al. [27] .

2.2 Problem development

In this section we have investigated steady, laminar, incompressible boundary layer magneto-hydrodynamic (MHD) flow of a nanofluid over non-linear stretching/shrinking permeable sheet. The sheet is moving with velocity $u_w = ax^m$, where a is constant, m is the power index and the wall mass suction/injection velocity is $v_w = v_w(x)$. We assume the co-ordinate system is taken as, x-axis along the sheet and y-axis perpendicular to the sheet The temperature of the surface of the sheet T_w is uniform and is greater than the ambient temperature T_∞, as $y \to \infty$, (i.e. $T_\infty < T_w$). Here, the magnetic $B(x)$ is to be connected along the y-direction by assuming electrical conducting nanofluids. The general equations for nanofluid are given below

$$\nabla.\mathbf{V} = 0, \tag{2.1}$$

$$\rho\frac{d\mathbf{V}}{dt} = \mathbf{J}\times\mathbf{B} + \boldsymbol{\nabla}.\boldsymbol{\tau}, \tag{2.2}$$

$$(\rho c)_{bf}(\mathbf{V}.\nabla T) = k\nabla^2 T + \tau.L + (\rho c)_p\left(D_B\nabla C.\nabla T + \frac{D_T}{T_\infty}(\nabla T)^2\right), \tag{2.3}$$

$$\mathbf{V}.\nabla C = \nabla\left(D_B\nabla C + \frac{D_T}{T_\infty}\nabla T\right). \tag{2.4}$$

In the above equations, ∇ stands for the differential operator, $\mathbf{V}$ the velocity vector, $\mathbf{J}$ the current density, $\boldsymbol{\tau}$ the Cauchy stress tensor, $\mathbf{J}\times\mathbf{B} = -\sigma B_0^2\mathbf{V}$ and $\mathbf{B} = \mathbf{B}_0 + \mathbf{b}$, the total magnetic field with applied magnetic field $\mathbf{B}_0$ and induced magnetic field $\mathbf{b}$. Here mathematically $\mathbf{V}$ and $\boldsymbol{\tau}$ termed as

$$\mathbf{V} = (u(x,y), v(x,y), 0), \tag{2.5}$$

$$\boldsymbol{\tau} = -p\mathbf{I} + \mu\mathbf{A_1}. \tag{2.6}$$

From above expression, μ the dynamic viscosity, p represents the pressure and $\mathbf{A_1}$ refers the first Rivlin-Ericksen tensor, as below

$$\mathbf{A_1} = \mathbf{L} + \mathbf{L}^T, \quad \text{where } \mathbf{L} = \nabla\mathbf{V}. \tag{2.7}$$

For velocity field $\mathbf{V} = (u(x,y), v(x,y), 0)$, the Lorentz force becomes

$$\mathbf{J} \times \mathbf{B} = -\sigma B_0^2 u\hat{\imath}. \tag{2.8}$$

Substituting the velocity field from Eq. (2.5), we have

$$\mathbf{L} = \begin{pmatrix} \frac{\partial u}{\partial x} & \frac{\partial u}{\partial y} & 0 \\ \frac{\partial v}{\partial x} & \frac{\partial v}{\partial y} & 0 \\ 0 & 0 & 0 \end{pmatrix}, \tag{2.9}$$

and

$$\mathbf{L}^T = \begin{pmatrix} \frac{\partial u}{\partial x} & \frac{\partial v}{\partial x} & 0 \\ \frac{\partial u}{\partial y} & \frac{\partial v}{\partial y} & 0 \\ 0 & 0 & 0 \end{pmatrix}. \tag{2.10}$$

When substituting Eqs. (2.9) and (2.10) in Eq. (2.7), we have

$$\mathbf{A_1} = \mathbf{L} + \mathbf{L}^T = \begin{pmatrix} 2\left(\frac{\partial u}{\partial x}\right) & \frac{\partial v}{\partial x} + \frac{\partial u}{\partial y} & 0 \\ \frac{\partial u}{\partial y} + \frac{\partial v}{\partial x} & 2\left(\frac{\partial v}{\partial y}\right) & 0 \\ 0 & 0 & 0 \end{pmatrix}. \tag{2.11}$$

Substituting Eqs. $(2.5) - (2.11)$ in Eqs. (2.1) and (2.2), the continuity and momentum equations in x and y directions give

$$\frac{\partial u}{\partial x} + \frac{\partial v}{\partial y} = 0, \tag{2.12}$$

$$u\left(\frac{\partial u}{\partial x}\right)+v\left(\frac{\partial u}{\partial y}\right)=\nu\left(2\frac{\partial^2 u}{\partial x^2}+\frac{\partial^2 u}{\partial y^2}+\frac{\partial^2 v}{\partial x\partial y}\right)-\frac{1}{\rho}\left(\frac{\partial p}{\partial x}\right)-\frac{\sigma B_0^2}{\rho}u, \tag{2.13}$$

$$u\frac{\partial v}{\partial x}+v\frac{\partial v}{\partial y}=\nu\left(\frac{\partial^2 v}{\partial x^2}+\frac{\partial^2 u}{\partial x\partial y}+2\left(\frac{\partial^2 v}{\partial y^2}\right)\right)-\frac{1}{\rho}\left(\frac{\partial p}{\partial y}\right). \tag{2.14}$$

Now by applying the boundary layer assumption, Eqs. (2.12) to (2.14) reduce to

$$\frac{\partial u}{\partial x}+\frac{\partial v}{\partial y}=0, \tag{2.15}$$

$$u\left(\frac{\partial u}{\partial x}\right)+v\left(\frac{\partial u}{\partial y}\right)=\nu\left(\frac{\partial^2 u}{\partial y^2}\right)-\frac{1}{\rho}\left(\frac{\partial p}{\partial x}\right)-\frac{\sigma B_0^2}{\rho}u. \tag{2.16}$$

The relevant boundary conditions are

$$u = Au_w(x), \qquad v=v_w, \qquad \text{at} \qquad y=0, \tag{2.17(a)}$$

$$u = 0, \qquad \text{as} \qquad y\to\infty. \tag{2.17(b)}$$

Under the boundary layer approach and using the boundary condition at infinity, the pressure gradient term can be termed as

$$-\frac{1}{\rho}\left(\frac{\partial p}{\partial x}\right)=0. \tag{2.18}$$

So, the momentum equation becomes

$$u\left(\frac{\partial u}{\partial x}\right)+v\left(\frac{\partial u}{\partial y}\right)=\nu\left(\frac{\partial^2 u}{\partial y^2}\right)-\sigma\frac{B^2}{\rho}u. \tag{2.19}$$

The energy and nanoparticle concentration equations are given below

$$(\rho c)_{bf}\left(u\left(\frac{\partial T}{\partial x}\right)+v\left(\frac{\partial T}{\partial y}\right)\right)=k\left(\frac{\partial^2 T}{\partial y^2}\right)+(\rho c)_p\left(D_B\left(\frac{\partial C}{\partial y}\right)\left(\frac{\partial T}{\partial y}\right)+\frac{D_T}{T_\infty}\left(\frac{\partial T}{\partial y}\right)^2\right)+\mu\left(\frac{\partial u}{\partial y}\right)^2, \tag{2.20}$$

$$u\left(\frac{\partial C}{\partial x}\right)+v\left(\frac{\partial C}{\partial y}\right)=D_B\left(\frac{\partial^2 C}{\partial y^2}\right)+\frac{D_T}{T_\infty}\left(\frac{\partial^2 T}{\partial y^2}\right). \tag{2.21}$$

The corresponding boundary conditions are

$$T = T_w, \quad D_B\left(\frac{\partial C}{\partial y}\right)+\frac{D_T}{T_\infty}\left(\frac{\partial T}{\partial y}\right)=0 \quad \text{at} \quad y=0, \tag{2.22(a)}$$

$$T \to T_\infty, \quad C=C_\infty \quad \text{as} \quad y\to\infty. \tag{2.22(b)}$$

In the above equations, u and$v$ represent the velocity components, μ the dynamic viscosity, k the thermal conductivity of the fluid, ν the kinematic viscosity, T the temperature of the fluid, ρ_{bf}, c_{bf} the density and specific heat of the basefluid respectively, and ρ_p, c_p the density and specific heat of the nanoparticle respectively. C the concentration of the nanoparticles,C_∞ the ambient nanoparticle concentration, D_T the thermal diffusion coefficient, D_B the Brownian diffusion coefficient and T_∞ the ambient temperature. Here, we have neglected the induced magnetic field.

Similarity transformations are introduced by the following relations

$$\begin{aligned} u &= ax^m f'(\eta), \quad v=-\sqrt{\frac{a\nu(m+1)}{2}}\left(x^{\frac{m-1}{2}}\right)\left[f(\eta)+\left(\frac{m-1}{m+1}\right)\eta f'(\eta)\right], \\ T &= T_\infty+(T_w-T_\infty)\theta(\eta), \quad \phi(\eta)=\frac{C-C_\infty}{C_\infty}, \quad \eta=y\sqrt{\frac{a(m+1)}{2\nu}}x^{\frac{m-1}{2}}. \end{aligned} \tag{2.23}$$

Hence, using the similarity variables, Eq. (2.1) is satisfied identically and the governing Eqs. (2.15) − (2.16) and (2.20) − (2.21) transform to:

$$f'''-\beta f'^2+ff''-Ha^2f'=0, \tag{2.24}$$

$$\theta''(\eta)+\Pr\left(Ecf''^2+f\theta'+Nt\theta'^2+Nb\theta'\phi'\right)=0, \tag{2.25}$$

$$\phi''+Lef\phi'+\frac{Nt}{Nb}\theta''=0. \tag{2.26}$$

The transformed boundary conditions are as follows:

$$f = s, \qquad f' = A, \qquad \theta = 1, \qquad Nb\phi' + Nt\theta' = 0 \qquad \text{at } \eta = 0, \tag{2.27(a)}$$

$$f' = 0, \qquad \theta = 0, \qquad \phi = 0 \qquad \text{at } \eta \to \infty. \tag{2.27(b)}$$

In the above equations, primes indicate differentiation with respect to η only, β is the power-law parameter, A the stretching/shrinking parameter, s the mass transfer parameter, Ha the Hartman number or magnetic field parameter, Nb, Nt the Brownian motion and thermophoresis parameters, respectively, Ec, Pr the Eckert and Prandtl numbers, respectively. All these are defined as:

$$\begin{aligned} \beta &= \frac{2m}{(m+1)}, \quad Ha = \sqrt{\frac{2\sigma B_0^2}{c\rho_f\,(m+1)}}, \quad s = -\frac{v_w}{\sqrt{\frac{av(m+1)}{2}}x^{(m-1)/2}}, \quad Ec = \frac{u_w^2\,(x)}{c_f\,(T_w - T\infty)}, \\ \Pr &= \frac{(\rho c)_f\,\nu}{k}, \quad Le = \frac{\nu}{D_B}, \quad Nt = \frac{(\rho c)_p\,D_T\,(T_w - T_\infty)}{(\rho c)_f\,\nu T_\infty}, \quad Nb = \frac{(\rho c)_p\,D_B C_\infty}{(\rho c)_f\,\nu}. \end{aligned} \tag{2.28}$$

The skin friction coefficient is defined by

$$C_f = \frac{\tau_w|_{y=0}}{\rho u_w^2} = \frac{\nu f''(0)\sqrt{\frac{a(m+1)}{2v}}}{ax^{(m+1)/2}}, \tag{2.29}$$

and

$$C_f\,\mathrm{Re}^{1/2} = f''(0). \tag{2.30}$$

The Nusselt number is given by

$$Nu_x = \frac{x\;q_w|_{y=0}}{k\,(T_w - T_\infty)} = -\theta'(0)\sqrt{\frac{a(m+1)}{2\nu}}x^{m+1/2}, \tag{2.31}$$

and

$$Nu_x\,\mathrm{Re}^{-1/2} = -\theta'(0). \tag{2.32}$$

Here $\mathrm{Re} = \left(\frac{u_w a(m+1)}{2\nu}\right)$ represents the Reynolds number.

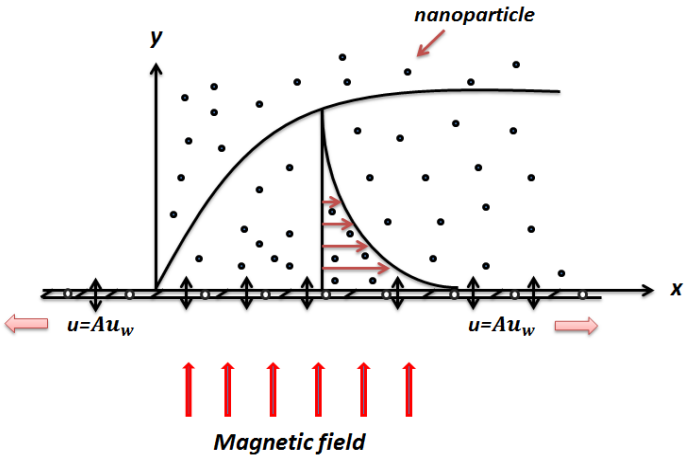

(a) Permeable stretching sheet ($A > 0$)

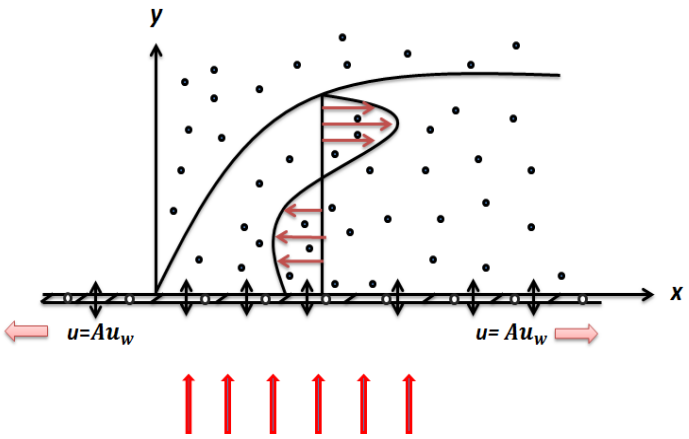

(b) Permeable shrinking sheet ($A < 0$)

Fig. 2.1: Physical sketch of the problem.

2.3 Result and discussion

The ordinary differential equations (2.24)-(2.26) with boundary conditions 2.27(a) and 2.27(b) can be solved numerically using bvp4c technique in Matlab software. The results are investigated numerically and reviewed in terms of the shear stress at the wall $f''(0)$, rate of heat transfer $\{-\theta'(0)\}$, velocity, temperature and nanoparticle concentration for different values of Hartmann number Ha, power law parameter β, mass transfer parameter s, Eckert number Ec, Prandtl number Pr, Lewis number Le, Brownian motion parameter Nb and thermophoresis parameter Nt, as shown in **Figs. 2.2** to **2.19**. To investigate this problem, we fixed default values for governing parameters as $\beta = 1.5$, $s = 3$, $Ha = 0.1$, Pr $= 5$, $Ec = 0.1$, $Le = 5$ and $Nt = Nb = 0.5$. In this chapter, we are interested in finding the dual solution, in which first solutions are displayed with solid lines and second solutions with dotted lines. We compared the skin friction $f''(0)$ and Nusselt number $\{-\theta'(0)\}$ with available published results in **Tables 2.1** to **2.3** decide the precision of our outcomes. A comparison of skin friction $f''(0)$ between exact and numerical solution are shown in **Table 2.4**. In the case of nanofluids, we compared the rate of heat transfer $\{-\theta'(0)\}$ of obtained results with earlier published results. The effect of Eckert number Ec and thermophoresis parameter Nt with default values of other parameters also shows the present results for the Nusselt number $\{-\theta'(0)\}$.

2.3.1 Effect of power law parameter

The effect of power law parameter β for the skin friction $f''(0)$, Nusselt number $\{-\theta'(0)\}$ and $\phi(0)$ against the suction parameter s shown in **Figs. 2.2** to **2.4**. In **Fig. 2.2**, first (upper) and second (lower) solutions of the skin friction $f''(0)$ are terminated by the critical value ($s_c = s$) i-e single solution, with increasing and decreasing behaviour against the suction parameter s respectively. The dual solution exist with respect to s for the range ($0 \leq \beta < 2$) without magnetic field ($Ha = 0$) and with magnetic field ($Ha = 0.2$). There is only one branch solution in both cases for $\beta < 0$. With increasing β, the critical value s_c increases. **Fig. 2.3** represents the Nusselt number with respect to power law parameter. It can be seen that the dual solution exist for positive value of β whereas there is only single solution for negative value of β. Both solutions of the rate of heat transfer bifurcate out of the single value i-e critical value

($s_c = s$) and the behaviour decreases with increasing β. From **Fig. 2.4**, the concentration of the nanoparticle at the wall $\phi(0)$ is pictured. Both solutions exist, as increases the value of power law parameter β but only single solution exist for ($\beta = -1$). Using default values of other parameters, for different values of β the magnitude of velocity profile shows (upper solution) decreases with β but the lower solution decreases with β in the boundary layer rigem upto $\eta \approx 1.5$ and after that a converse behaviour is noticed (see **Fig. 2.5**).

2.3.2 Effect of Hartmann number

The effect of Hartmann number (magnetic field) Ha on skin friction $f''(0)$, nanoparticle concentration $\phi(0)$, Nusselt number $\{-\theta'(0)\}$ and velocity profile $f'(\eta)$ has been captured (see **Figs. 2.6** to **2.9**). In the absence ($Ha = 0$) and presence ($Ha = 0.2$) of magnetic field the dual solution are sketched. The critical value s_c is changing with Ha. In **Fig. 2.6**, it can be observed that as increasing in magnetic field Ha (0 to 0.6), the critical value s_c reduces from (2.1361 to 1.7991). Similar observation are also seen for the concentration of nanoparticle and Nusselt number. As increasing in magnetic field Ha, the skin friction $f''(0)$ increases but the nanoparticle concentration at the surface $\phi(0)$ reduces.

2.3.3 Effect of viscous dissipation

Fig. 2.10 illustrates the effect of viscous dissipation on the rate of heat transfer $\{-\theta'(0)\}$ for different values of s keeping default values of other parameters. The dual solution has been plotted and seen that with the effect of viscous dissipation the critical values s_c close to same. Viscous dissipation which is characterized by Eckert number Ec, is the ratio of kinetic energy and enthalpy. The temperature rises in the boundary layer regime for increasing value of Ec. So in **Fig. 2.10** the rate of heat transfer decreases with Ec. It can be noticed that the first solution is higher as compared to the second in the absence of viscous effect ($Ec = 0$), but there is an opposite trend at ($Ec = 0.1$).

2.3.4 Effect of stretching/shrinking and mass transfer parameter

From **Figs. 2.11** to **2.12**, for various values of mass transfer parameter ($s > 0$) the skin friction and Nusselt number are sketched with respect to stretching/shrinking parameter A. The dual

solution of the skin friction and Nusselt number has been plotted for $s = 3$, 3.5. The critical value A_c is varying with s. It is illustrated as mass transfer parameter s increases from 3.0 to 3.5**,** A_c decreases from -1.9792 to -2.6909. Thus, it can be noticed that the skin fraction and Nusselt number rises with rising the mass transfer parameter s.

From **Fig. 2.13**, the dual solution are plotted for $s \geq 2.2$ for velocity profile. The magnitude of velocity is rises in the upper branch solution and reduces in the lower branch solution as mass transfer parameter s increases. It can likewise be watched that of both solutions more will be the partition with the enlargement of s.

2.3.5 Effect of nanofluid parameters

In **Fig**. **2.14**, the effect of Brownian motion parameter Nb on concentration of nanoparticle $\phi(\eta)$ demonstrates that the enlargement of Nb decreases the nanoparticle concentration. The gradient of nanoparticle concentration at the surface is controlled passively at the surface by product of $\left(-\frac{Nt}{Nb}\right)$ and temperature gradient. So the nanoparticle concentration gradient rises with Nt and reduces with Nb. The effect of thermophoresis parameter Nt on non-dimensional temperature $\theta(\eta)$ and nanoparticle concentration $\phi(\eta)$ has been discussed in **Figs. 2.15** and **2.16** keeping other parameters fixed. **Table 2.5** shows the rate of heat transfer $\{-\theta'(0)\}$ decreases with enlargement in thermophoresis parameter Nt.

2.3.6 Effect of Prandtl and Lewis numbers

From **Figs**. **2.17** and **2.18**, the variation of non-dimensional temperature $\theta(\eta)$ and nanoparticle volume friction $\phi(\eta)$ has been discussed with Pr, taking other parameters fixed. The two solutions are sketched for various values of Pr. The ratio of momentum diffusivity and thermal diffusivity is named as Prandtl number. So for $\mathrm{Pr} > 1$, the momentum boundary layer thickness is greater than the thermal boundary layer thickness. The non-dimensional temperature $\theta(\eta)$ is decreases as Prandtl number Pr increases (see **Fig**. **2.17**). In **Fig. 2.18**, the concentration of nanoparticle ascends near the surface with the enlargement of Prandtl number Pr while after a certain distance it tumbles down far from the surface. The temperature profile is diminishing with increases in Pr. From **Fig. 2.19(a),** the Nusselt number $\{-\theta'(0)\}$ is increasing with increasing in Prandtl number Pr.

In **Fig. 2.19(b)**, the effect of Lewis number Le on $\{-\theta'(0)\}$ has been investigated, keeping other parameters fixed. More than one solution is plotted. The ratio of thermal diffusivity to mass diffusivity is termed as Lewis number. So the thermal boundary layer thickness is greater than the nanoparticle boundary layer thickness for $Le > 1$. It can be seen that in **Fig. 2.19,** the Nusselt number $\{-\theta'(0)\}$ is lower for higher value of Lewis number Le.

Table 2.1: Values for skin friction $f''(0)$ for different values of power-index m, when $Ha = 0 = s$ and $A = 1$(stretching sheet).

m	Cortall[28]	Javid at al. [29]	Abbas and Hayat [30]	Present results
0.0	0.62754	0.627554	0.627547	0.627556
0.2	0.76675	0.766837	0.76683	0.766837
0.5	0.88947	0.889543	0.889544	0.889543
1.0	1.00000	1.00000	1.00000	1.00000
1.5	1.06158	1.06160	1.061601	1.06160
3.0	1.14858	1.14859	1.148593	1.14860
7.0	1.21684	1.21685	1.216851	1.21685
10.0	1.23487	1.234875	1.234874	1.23488
20.0	1.25741	1.25742	1.257423	1.25743
100.0	1.27676	1.27677	1.276773	1.27678

Table 2.2: Comparison of $\{-\theta'(0)\}$ for different values of Pr and power-index m when $Ha = 0 = s = Le$, $Ec = 0.1$, $A = 1$.

Pr	m	Cortall[28]	Javid at al. [29]	Abbas and Hayat [30]	Present results
1.0	0.2	0.574985	0.575268	0.574955	0.575268
	0.5	0.556623	0.556776	0.556775	0.556776
	1.5	0.530966	0.530962	0.530962	0.530966
	3.0	0.517977	0.518034	0.518043	0.518035
	10.0	0.505121	0.505327	0.505127	0.505328
5.0	0.2	1.474764	1.475036	1.474203	1.47504
	0.5	1.436789	1.437028	1.437242	1.43703
	1.5	1.381861	1.382088	1.382003	1.38209
	3.0	1.352768	1.353763	1.352548	1.35378
	10.0	1.324772	1.3254	1.324943	1.32542

Table 2.3: Comparison of $\{-\theta'(0)\}$ for different values of Ec, Pr and Ha when $Le = 0$, $A = -1$ (shrinking case).

Ec	Pr	$Ha = 0$		$Ha = 0.5$	
		Javid at al. [29]	Present results	Javid at al. [29]	Present results
0.0	0.7	1.9624	1.94254	1.9659	1.94664
	1.0	2.815	2.81082	2.8191	2.81503
	3.0	8.7295	8.72933	8.7324	8.73227
	7.0	20.6953	20.6952	20.6968	20.6968
	10.0	29.6869	29.6868	29.6881	29.6880
	20.0	–	59.6768	–	59.6775
0.1	0.7	1.8717	1.85164	1.8715	1.85187
	1.0	2.6843	2.68041	2.6829	2.67909
	3.0	8.3323	8.3363	8.3191	8.31993
	7.0	19.7637	19.7672	19.7276	19.7299
	10.0	28.3544	28.3595	28.3016	28.3572
	20.0	–	57.0180	–	56.9070

Table 2.4: Comparison of the skin friction $f''(0)$ between numerical and exact solutions for $A = -1$(shrinking sheet) with $\beta = 1$.

s	m	Exact solution [31]		Present results	
		First solution	Second solution	First solution	Second solution
3.0	0.1	2.622497	0.377503	2.6225	0.377503
	0.3	2.657584	0.342416	2.65758	0.342416
	0.5	2.724745	0.275255	2.72474	0.275255
4.0	0.1	3.734935	0.265065	3.73494	0.265065
	0.3	3.75784	0.24216	3.75784	0.24216
	0.5	3.802776	0.197224	3.80278	0.197224

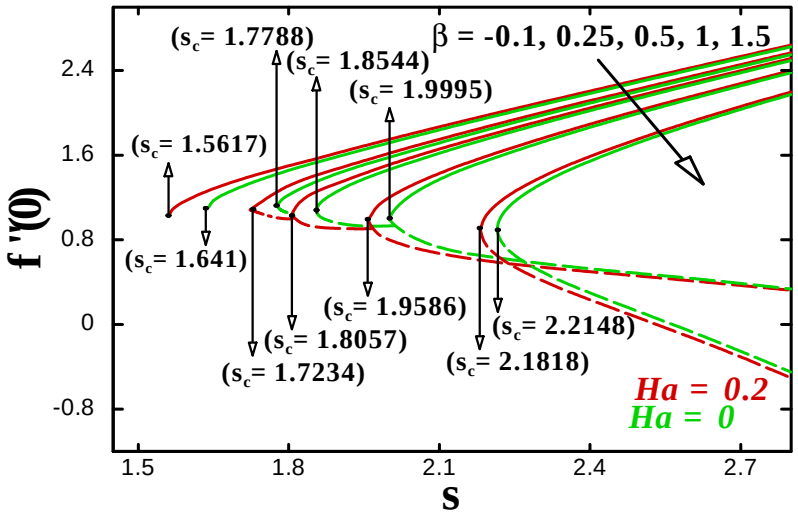

Fig. 2.2: The effect of power law parameter β on the wall shear stress $f''(0)$.

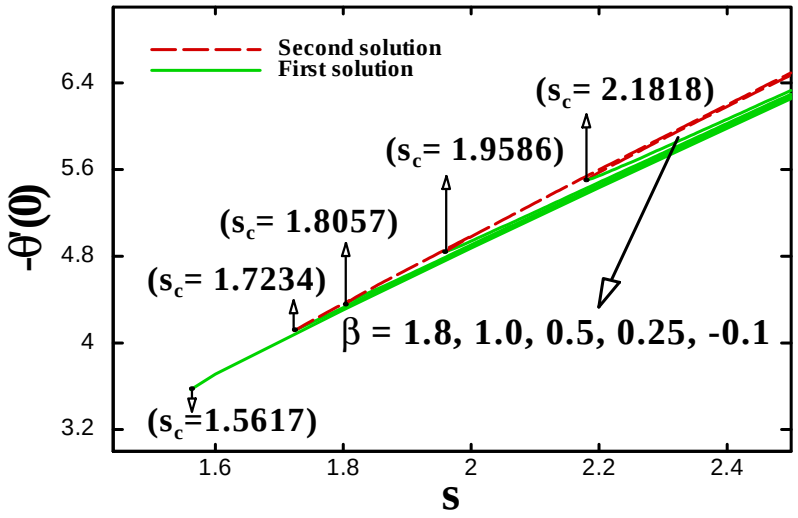

Fig 2.3: variation of $\{-\theta'(0)\}$ on mass transfer parameter s when $Ha = 0.2$.

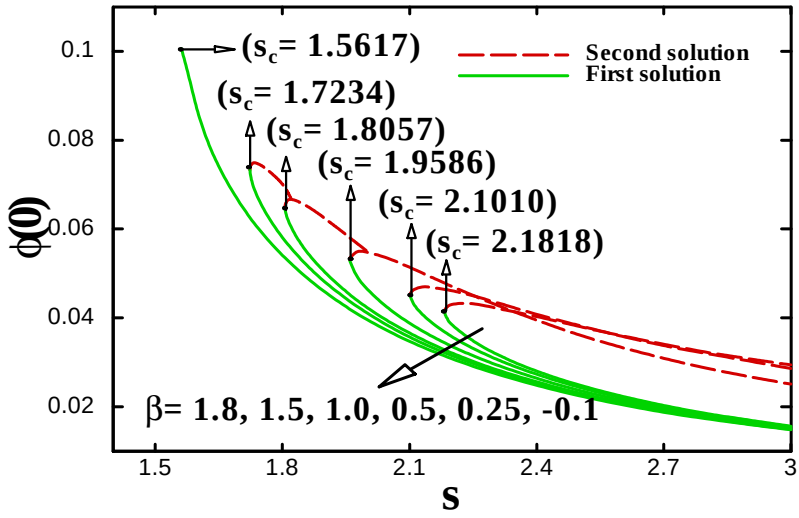

Fig 2.4: The effect of power-law parameter β on nanoparticle concentration at the wall $\phi(0)$ when $Ha = 0.2$.

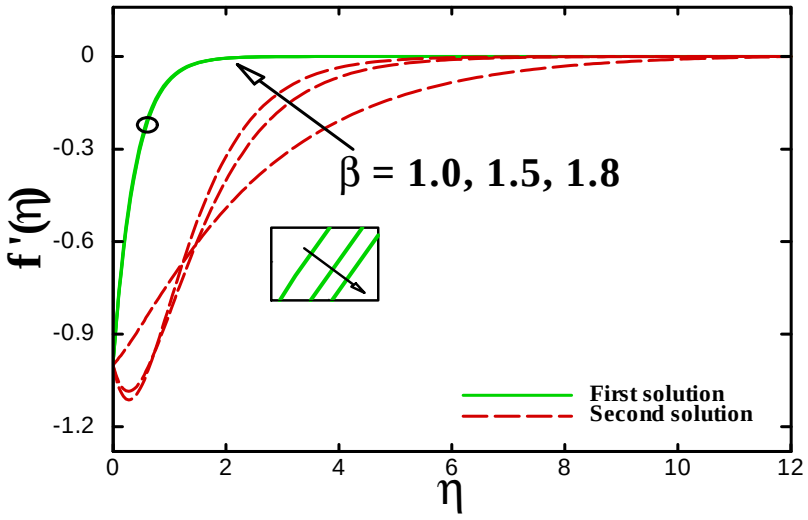

Fig 2.5: Velocity distribution $f'(\eta)$ for various values of power-law parameter β.

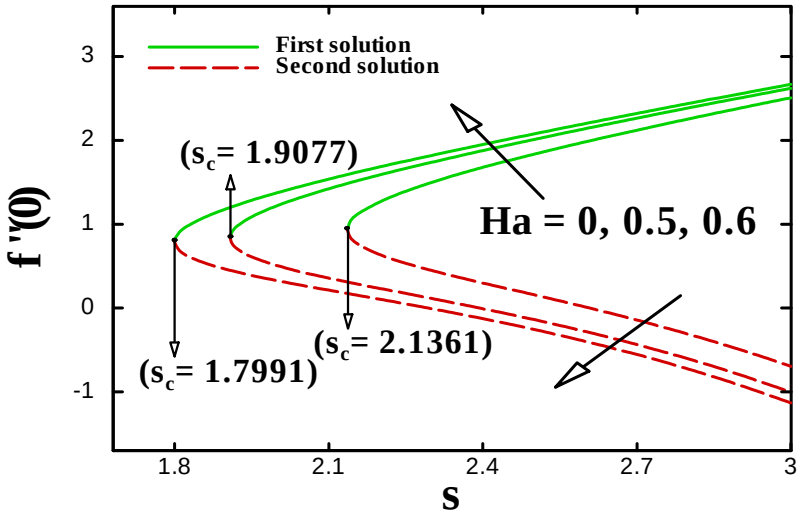

Fig 2.6: The effect of Hartmann number (magnetic field parameter) Ha on the shear stress at the wall $f''(0)$ for various values of mass transfer parameter s.

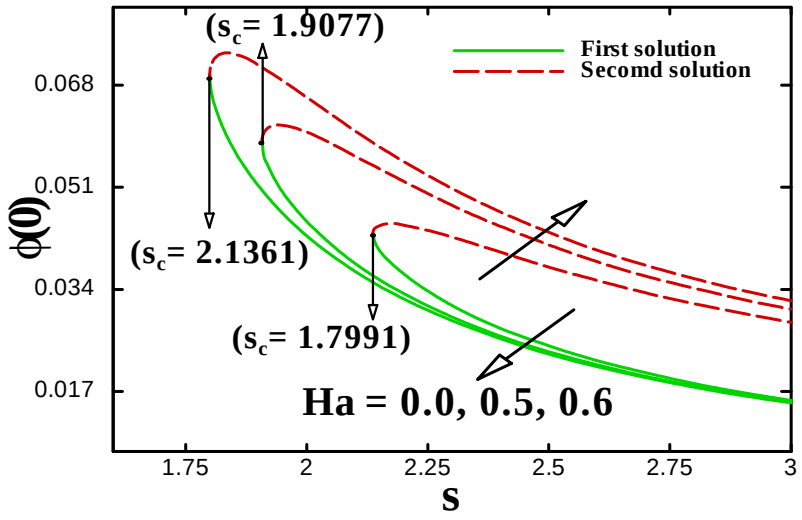

Fig. 2.7: Variation of nanoparticle concentration at the wall $\phi(0)$ for different values of magnetic field Ha.

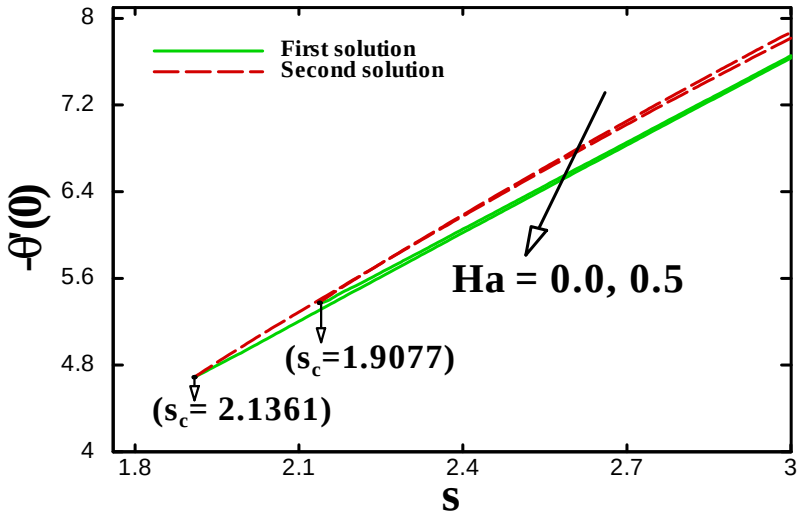

Fig 2.8: Variation of the rate of heat transfer at the wall $\{-\theta'(0)\}$ on the mass transfer parameter s.

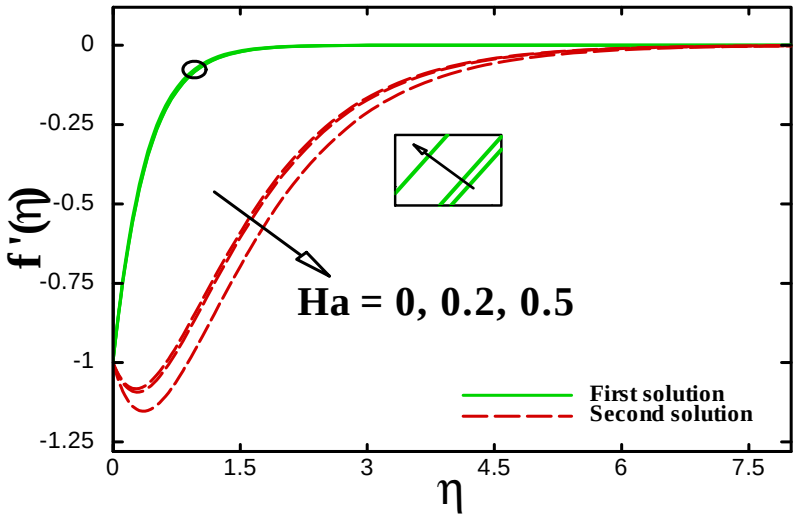

Fig. 2.9: Velocity profile $f'(\eta)$ for different values of Hartmann number Ha.

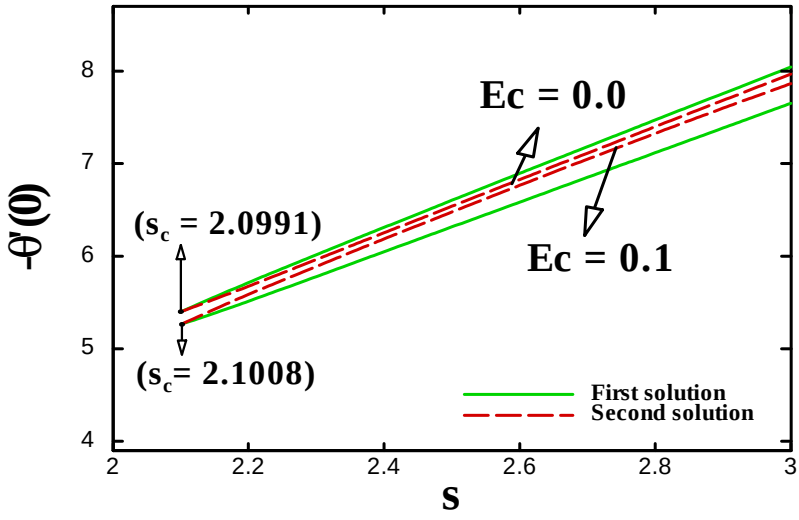

Fig. 2.10: The effect of Eckert number Ec on the rate of heat transfer $\{-\theta'(0)\}$ when $Ha = 0.2$.

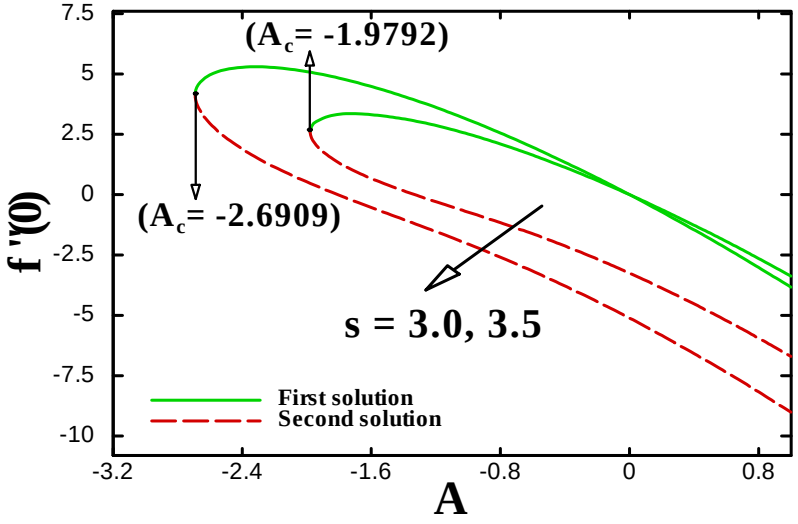

Fig. 2.11: Variation of the skin friction $f''(0)$ on A.

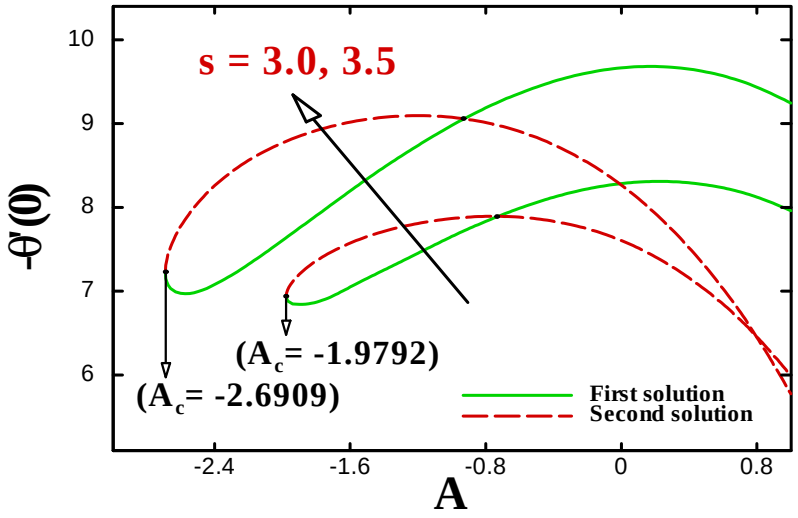

Fig. 2.12: The effect of stretching/shrinking parameter A on $\{-\theta'(0)\}$.

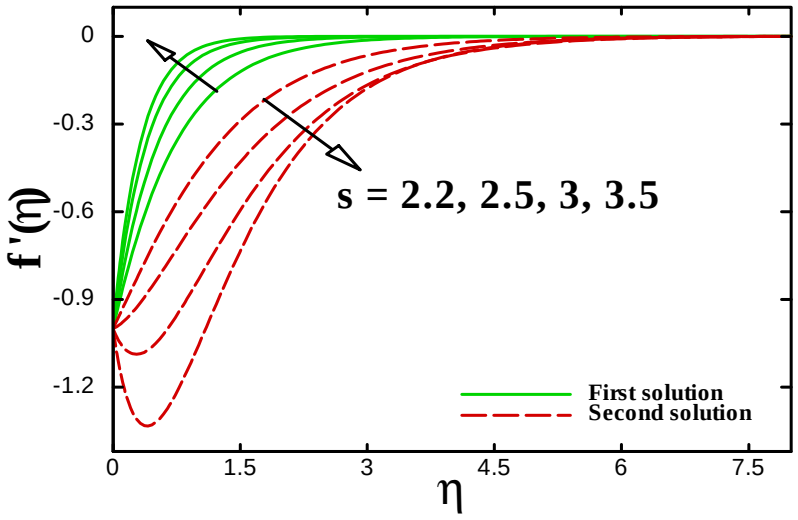

Fig. 2.13: Velocity profile $f'(\eta)$ for different values of mass transfer parameter s.

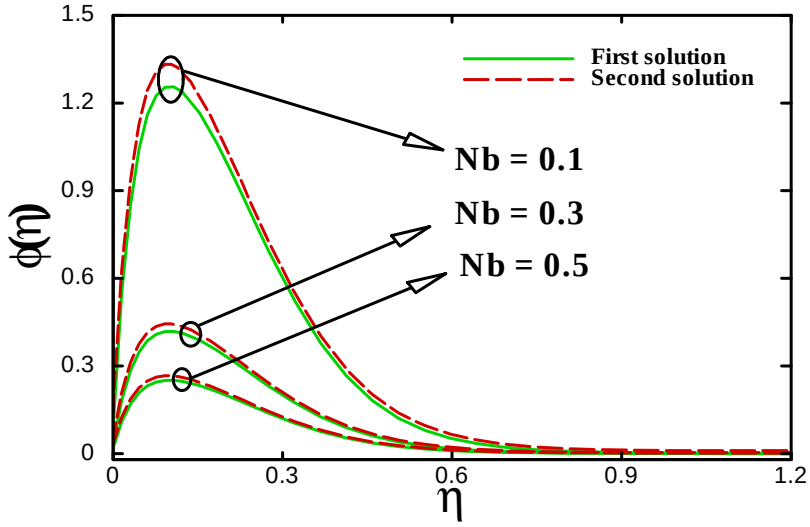

Fig. 2.14: Nanoparticle concentration profile $\phi(\eta)$ with Brownian motion parameter Nb.

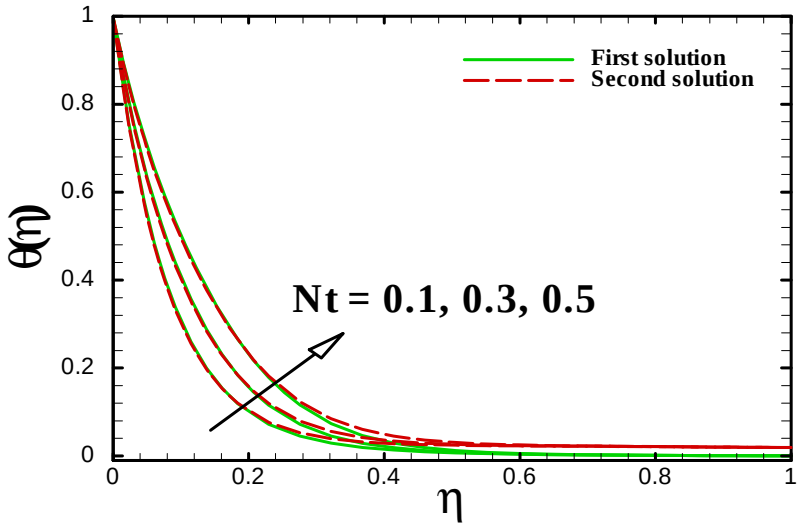

Fig. 2.15: Temperature profile $\theta(\eta)$ with thermophoresis parameter Nt.

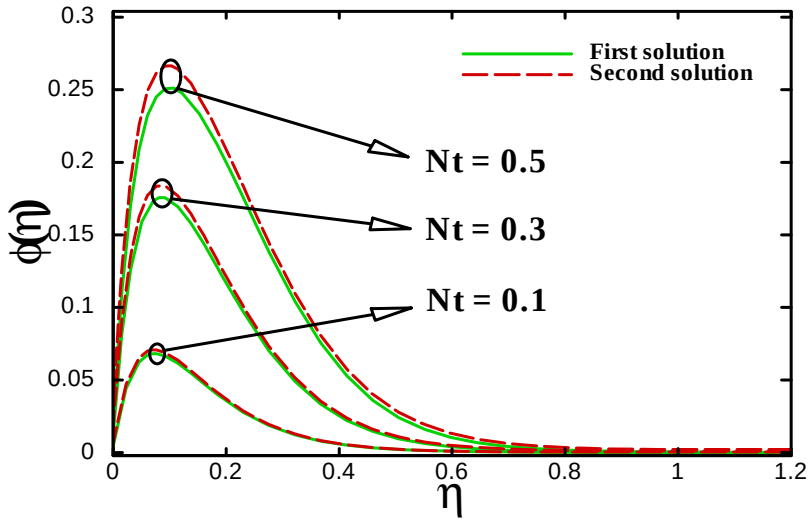

Fig. 2.16: The effect of Brownian motion parameter Nb on concentration profile of nanoparticle $\phi(\eta)$.

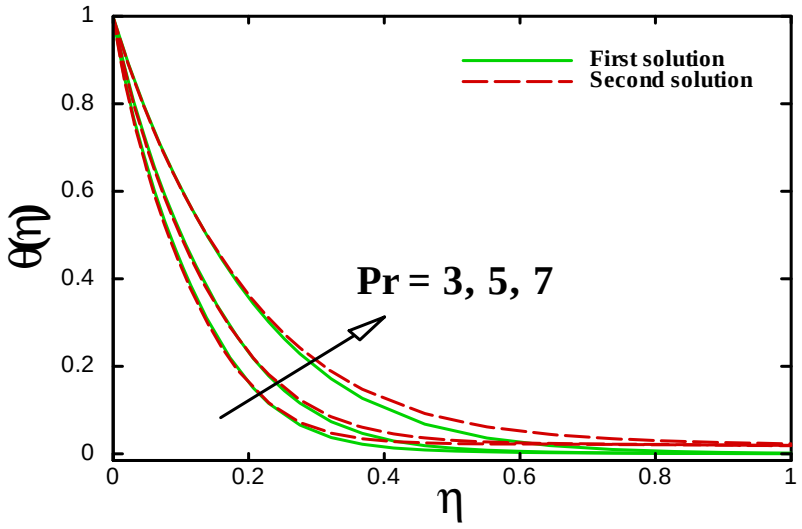

Fig. 2.17: Temperature profile $\theta(\eta)$ with Prandtl number Pr.

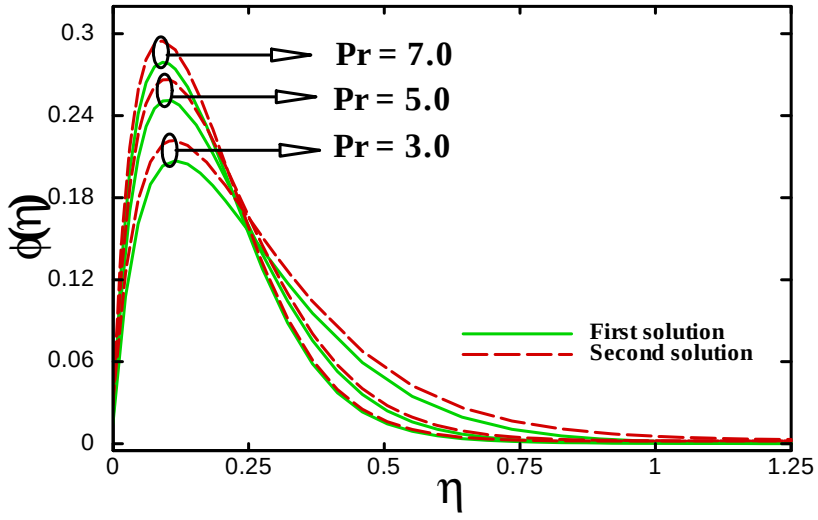

Fig. 2.18: The effect of Prandtl number Pr on concentration profile of nanoparticle $\phi(\eta)$.

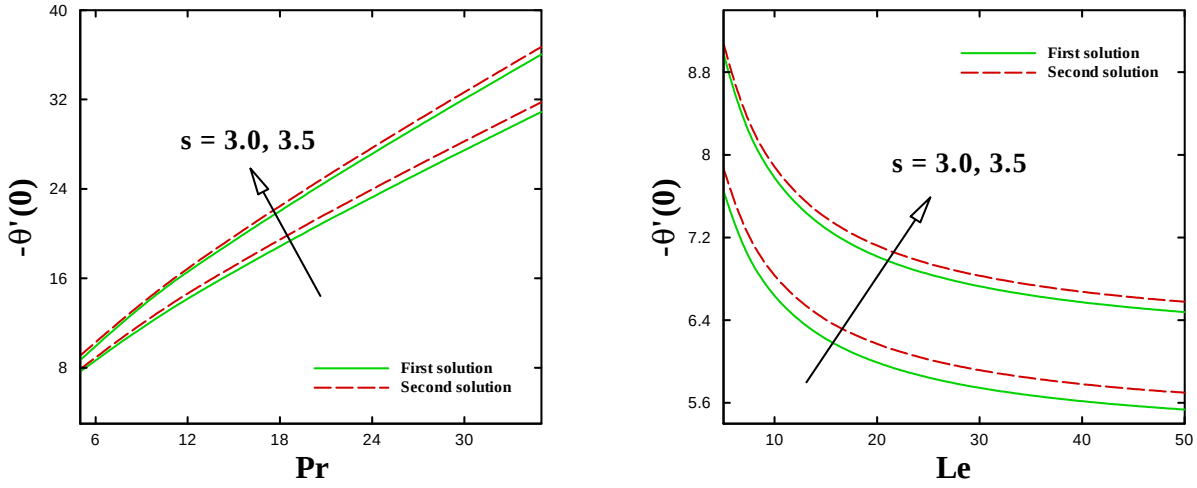

Fig. 2.19: Variation of Nusselt number $\{-\theta'(0)\}$ with Pr and Le for various value of mass transfer parameter s.

Table 2.5: Numerical values of the Nusselt number $\{-\theta'(0)\}$ for various values of Ha, Ec and Nt, in the case of shrinking sheet $A = -1$ when $\beta = 1.5$, $s = 3.0$, $Le = 5.0 = \Pr$ and $Nb = 0.5$.

Ha	Ec	Nt	Upper solution	lower solution
0.0	0.0	0.1	12.955497	12.882934
		0.3	10.12651	10.050836
		0.5	8.0439777	7.9695368
	0.1	0.1	12.37714	12.61308
		0.3	9.6671463	9.8895352
		0.5	7.8732234	7.8732234
0.2	0.0	0.1	12.955859	12.881651
		0.3	10.126843	10.049483
		0.5	8.0443398	7.9682024
	0.1	0.1	12.373103	12.598269
		0.3	9.6634519	9.8792321
		0.5	7.6511463	7.8656952

2.4 Conclusions

The basic goal of this chapter has been to investigate the dual solution of MHD boundary layer flow over stretching/shrinking sheet of nanofluid. We have used the similarity variables to convert the non-linear partial differential equations into ordinary differential equations. Moreover, we have solved the ordinary differential equations with bvp4c function in Matlab. Results for the skin friction $f''(0)$, Nusselt number $\mathrm{Re}^{-1/2}\, Nu_x$, nanoparticle volume friction at the surface $\phi(0)$, velocity $f'(\eta)$, temperature $\theta(\eta)$ and nanoparticle volume friction $\phi(\eta)$ profiles are described. Some of the findings are summarized below.

- For the existence of both first and second solution, the critical values (s_c and A_c) are found.
- It is seen that skin friction decreases whereas, Nusselt number and nanoparticle concentration at the wall increase with increasing value of power law parameter β.
- At the surface, the first solution of the skin friction increases whereas, for Nusselt number and nanoparticle concentration it decrease with magnetic field Ha.
- The non-dimensional temperature increases with increase in thermophoresis parameter Nt.
- The non-dimensional nanoparticle concentration $\phi(\eta)$ reduces with Nb but rises with the increasing value of Nt.

Chapter 3

A study on slip-flow and heat transfer performance of nanofluid from a permeable shrinking surface with thermal radiation: Dual solution

3.1 Introduction

The reason for this chapter is to augment the investigation examined in chapter 2. In this chapter we investigate a computational study on the stagnation-point flow of an electrically conducting nanofluids over a non-linear stretching/shrinking surface with first-order slip. The analysis of heat transfer on the flow field is also performed in the presence of non-linear thermal radiation. The same numerical technique as in chapter 2 is utilized. The obtained numerical solutions are presented graphically and some interesting results like multiple (upper and lower) solutions are found. The critical values corresponding to the suction parameter s and the shrinking parameter A are computed. The effect of different dimensionless parameters like as power-law parameter, Hartmann number, slip parameter, Eckert number, temperature ratio

parameter, radiation parameter, Brownian motion and thermophoresis parameters and Lewis number are examined and displayed graphically. The dimensionless slip parameter has a reducing impact on the skin friction coefficient for the upper branch solutions. The major outcome of the present study is that the temperature ratio parameter boosts the temperature profiles for both solutions. While the temperature profiles show a decreasing behaviour for higher non-linear radiation parameter. Validation of numerical scheme is accomplished by means of benchmarking with some already reported studies, and a great correlation is illustrated.

3.2 Problem development

Let us assume an incompressible, two-dimensional stagnation-point flow of nanofluid towards a nonlinear stretching/shrinking sheet. The heat and mass transfer is studied under the influence of nonlinear thermal radiation and viscous dissipation. We assumed that the sheet is moving with the velocity $u_w(x) = ax^m$ and the velocity of the wall mass suction/injection is $v_w(x) = x^m$, where a is constant. We assume the coordinate system is taken as, x-axis along the sheet and y-axis perpendicular to the sheet. The fluid is moving due to the equal and opposite forces, which are applied along the x-axis towards the origin 'O' of the coordinate system, so that the wall shrinks keeping the origin fixed, under the influence of nonlinear stretching/shrinking of the sheet. Here $u_w(x) < 0$ corresponds to a shrinking/contracting surface sheet velocity and $u_w(x) > 0$ corresponds to a stretching surface sheet velocity. The temperature T_w of the surface of the sheet is uniform and is greater than the ambient temperature T_∞, as $y \to \infty$, (i.e. $T_\infty < T_w$). Here, it is assumed to be applied the variable magnatic field $B(x)$ along the y-direction, by assuming electrical conducting nanofluids. The ambient nanoparticle volume fraction is C_∞. Under these assumptions, the steady conservation of mass, momentum equation, energy and nanoparticle fraction equations for nanofluid with boundary layer approximations are presented in Cartesian coordinates as:

$$\frac{\partial u}{\partial x} + \frac{\partial v}{\partial y} = 0, \tag{3.1}$$

$$u\left(\frac{\partial u}{\partial x}\right) + v\left(\frac{\partial u}{\partial y}\right) = \nu\left(\frac{\partial^2 u}{\partial y^2}\right) + u_e\left(\frac{du_e}{dx}\right) - \frac{\sigma B_0^2}{\rho}\left(u - u_e\right), \tag{3.2}$$

$$(\rho c)_{bf}\left(u\left(\frac{\partial T}{\partial x}\right)+v\left(\frac{\partial T}{\partial y}\right)\right)=k\left(\frac{\partial^2 T}{\partial y^2}\right)+(\rho c)_p\left(D_B\left(\frac{\partial C}{\partial y}\right)\left(\frac{\partial T}{\partial y}\right)+\frac{D_T}{T_\infty}\left(\frac{\partial T}{\partial y}\right)^2\right)-\frac{\partial q_r}{\partial y}+\mu\left(\frac{\partial u}{\partial y}\right)^2, \tag{3.2}$$

$$u\left(\frac{\partial C}{\partial x}\right)+v\left(\frac{\partial C}{\partial y}\right)=D_B\left(\frac{\partial^2 C}{\partial y^2}\right)+\frac{D_T}{T_\infty}\left(\frac{\partial^2 T}{\partial y^2}\right). \tag{3.4}$$

Here u and v are the velocity components in x and y directions, respectively, μ the dynamic viscosity, ν the kinematic viscosity, k the thermal conductivity of the fluid, T the temperature of the fluid, ρ_{bf}, c_{bf} the density and specific heat of the basefluid respectively, and ρ_p, c_p the density and specific heat of the nanoparticle respectively. C the concentration of the nanoparticles, T_∞ is the ambient temperature, D_B and D_T the Brownian and thermal diffusion coefficient.

With an assumption for the optically thick boundary layer we adopt Rosseland's diffusion approximation [32] for the radiative heat flux q_r and the expression is given by

$$q_r=-\frac{4\sigma^*}{3k^*}\frac{\partial T^4}{\partial y}=-\frac{16\sigma^*}{3k^*}T^3\frac{\partial T}{\partial y}. \tag{3.5}$$

whereas, k^* and σ^* indicate the mean absorption and the Stefan-Boltzmann constant, respectively.

The relevant boundary conditions are:

$$\begin{aligned} u &= Au_w(x)+u_{slip}, \quad v=v_w, \quad T=T_w, \quad D_B\frac{\partial C}{\partial y}+\frac{D_T}{T_\infty}\frac{\partial T}{\partial y}=0 \quad \text{at} \quad y=0, \\ u &= u_e(x)=cx^m, \qquad T\to T_\infty, \qquad C=C_\infty \quad \text{as} \quad y\to\infty. \end{aligned} \tag{3.6}$$

In formulation of Eq. (3.2), we have neglected the induced magnetic field. We assume the partial slip at the wall and the slip velocity has the form $u_{slip}=L\frac{\partial u}{\partial y}$, where L stands for the velocity slip factor. The boundary condition $D_B\left(\frac{\partial C}{\partial y}\right)+\frac{D_T}{T_\infty}\left(\frac{\partial T}{\partial y}\right)=0$ at $y=0$ in Eq. (3.6) shows the normal flux of nanoparticles is zero at the boundary with consideration of thermophoresis, (see Kuznetsov and Nield [33]).

We introduce the following locally similarity transformations for equations (3.1) - (3.4) with

boundary conditions (3.6):

$$\begin{aligned}\eta &= y\sqrt{\frac{a(m+1)}{2\nu}}\left(x^{\frac{m-1}{2}}\right), \qquad \theta(\eta)=\frac{T-T_\infty}{T_w-T_\infty}, \qquad \phi(\eta)=\frac{C-C_\infty}{C_\infty},\\ u &= cx^m f'(\eta), \qquad v=-\sqrt{\frac{a\nu(m+1)}{2}}\left(x^{(m-1)/2}\right)\left[f(\eta)+\frac{m-1}{m+1}\eta f'(\eta)\right]. \end{aligned} \tag{3.7}$$

We designate the non-dimensional temperature $\theta(\eta)=\frac{T-T_\infty}{T_w-T_\infty}$ with $T=T_\infty\left(1+(\theta_w-1)\theta\right)$, whereas, $\theta_w=\left(\frac{T_w}{T_\infty}\right)$, $\theta_w\,(>1)$ being the temperature ratio parameter.

Hence, using the similarity variables (3.7), Eq. (3.1) is satisfied identically and the governing Eqs. $(3.2)-(3.4)$ transform to:

$$f'''+ff''+\beta\left(1-f'^2\right)+Ha^2\left(1-f'\right)=0, \tag{3.8}$$

$$\frac{d}{d\eta}\left[\left(1+\frac{4}{3Nr}\{1+(\theta_w-1)\theta\}^3\right)\theta'\right]+\Pr\left(Ecf''^2+f\theta'+Nt\theta'^2+Nb\theta'\phi'\right)=0, \tag{3.9}$$

$$\phi''+Lef\phi'+\left(\frac{Nt}{Nb}\right)\theta''=0. \tag{3.10}$$

The transformed boundary conditions are as follows:

$$\begin{aligned} &f=s, \qquad f'=A+\alpha f'', \qquad \theta=1, \qquad Nb\phi'+Nt\theta'=0 \qquad \text{at } \eta=0,\\ &f'=1, \qquad \theta=0, \qquad \phi=0 \qquad \text{at } \eta\to\infty. \end{aligned} \tag{3.11}$$

In the above equations, prime refers differentiation with respect to η, β the power-law parameter, A the stretching/shrinking parameter, α the velocity slip parameter, s the mass transfer parameter, Ha the Hartmann number or magnetic field parameter, Nr is the radiation parameter, Nb, Nt the Brownian motion and thermophoresis parameters, respectively, $Ec, \Pr$ the

Eckert and Prandtl numbers, respectively. These are defined as:

$$\begin{aligned}
\beta &= \frac{2m}{m+1}, \qquad Ha = \sqrt{\frac{2\sigma B_0^2}{c\rho_f\,(m+1)}}, \qquad s = -\frac{v_w}{\sqrt{\frac{a\nu(m+1)}{2}}\left(x^{(m-1)/2}\right)}, \\
Ec &= \frac{u_w^2\,(x)}{c_f\,(T_w - T\infty)}, \qquad \Pr = \frac{(\rho c)_f\,v}{k}, \qquad \alpha = L\sqrt{\frac{a\,(m+1)}{2\nu}}\left(x^{(m-1)/2}\right), \\
Le &= \frac{\nu}{D_B}, \qquad Nt = \frac{(\rho c)_p\,D_T\,(T_w - T_\infty)}{(\rho c)_f\,\nu T_\infty}, \qquad Nb = \frac{(\rho c)_p\,D_B C_\infty}{(\rho c)_f\,\nu}.
\end{aligned} \tag{3.12}$$

3.2.1 Parameters of physical interest

We are intended in the physical quantities, as the skin friction coefficient C_f and the local Nusselt number Nu_x, respectively. Whereas τ_w is the wall shear stress and q_w represents the wall heat flux. Conventionally, these are defined as:

$$C_f = \frac{\tau_w}{\rho u_w^2}, \qquad Nu_x = \frac{x q_w}{k\,(T_w - T_\infty)}. \tag{3.13}$$

in which:

$$\tau_w = \mu\left(\frac{\partial u}{\partial y}\right)\Big|_{y=0}, \qquad q_w = -k\left(\frac{\partial T}{\partial y}\right)\Big|_{y=0} + q_r|_{y=0}\,. \tag{3.14}$$

Using the similarity Eq. (3.7) into Eq. (3.13) , we get the corresponding expressions:

$$\mathrm{Re}^{1/2}\,C_f = f''(0), \quad \mathrm{Re}^{-1/2}\,Nu_x = -\left(1 + \frac{4}{3N_r}\right)\theta'(0), \tag{3.15}$$

whereas the local Reynolds number and is defined as $\mathrm{Re} = \frac{a}{\nu}\frac{m+1}{2}x^{(m+1)}$.

Due to new mass flux condition $Nb\phi'(0) + Nt\theta'(0) = 0$, the Sherwood number is obtained identically zero, (see Kuznetsov and Nield [33]).

3.3 Results and discussion

To investigate the present problem, we fix the default values of governing parameters by using numerical approach as, $\beta = 1.0$, $Ha = 0.1$, $A = -1.1$, $\alpha = 0.1$, $\theta_w = 1.1$, $Nr = 1.1$, $\Pr = 1.05$, $Ec = 0.1$, $Nt = 0.1$, $Nb = 0.1$. The effect of given parameters on skin friction $f''(0)$, Nusselt Number $\mathrm{Re}^{-1/2}\,Nu_x$, velocity $f'(\eta)$, temperature $\theta(\eta)$ and nanoparticles concentration $\phi(\eta)$ are

presented graphically for different values of governing parameters. In this chapter we consider the dual solution, in which first solution is displayed with solid lines and the second solution with dotted lines.

To find out the precision of the numerical results gotten through the bvp4c scheme, a comparison of skin friction coefficient $f''(0)$ is made for limiting cases (in the absence of magnetic field and suction) and no-slip condition. These comparison can be found in **Tables 3.2** and **3.3** with those of Wang [34] , Yacob and Ishak [35] and Gorla et al. [36] for various values of shrinking parameter A. These tables demonstrate a decent assertion between the present numerical results and the past outcomes. This gives us reliance of our numerical outcomes.

The variations of physically important quantities like skin friction coefficient $f''(0)$, Nesselt number $\mathrm{Re}^{-1/2}\, Nu_x$ and nanoparticles concentration at the wall $\phi(0)$ are respectively presented through **Figs**. **3.1** to **3.3** to see the impact of different pertinent flow parameters. The key factor of this analysis is that, we captured the dual solution i.e. (two branches). These two solutions are commonly known as first and second solutions or (upper and lower branch), respectively. These dual solution are achieved in case of flow over a shrinking surface in the presence of mass suction.

Fig. **3.1** discloses the effect of power-law parameter β on the skin friction coefficient in terms of $f''(0)$ in case of no-slip and partial-slip surface conditions. For both the situations, the critical values A_c corresponding to several values of power-law parameter are listed in this figure. It is seen that for mass suction ($s = 3$), the magnitude of critical values $|A_c|$ expands with increasing values of power-law parameter. Consequently, more increment in power-law parameter β will cause an expansion in the existence domain of dual solution. Moreover, these effects are much higher in case of partial slip condition i.e., ($\alpha = 0.1$) which means that the range of the values of A for which the dual solution of the boundary layer equations exists, are higher. This is further reflected in both figures that the first solution for skin friction is always higher than the second. Moreover, the skin friction coefficient decreases with the enlargement of β. The variations of the local Nusselt number $\mathrm{Re}^{-1/2}\, Nu_x$ against A for power-law parameter $\beta = 0.8, 1.0, 1.8$ without velocity-slip ($\alpha = 0$) and with velocity-slip ($\alpha = 0.1$) are shown in **Fig**. **3.2** respectively. As indicated by our computations in this chapter, it is clear from these figures that dual solutions exist in the range $A_c(= -4.162, -4.386, -4.4425) \leq A \leq 1.5$ in case

of no-slip effects and $A_c(= -4.8498, -5.1888, -5.28) \leq A \leq 1.5$ for velocity–slip effects when $\beta = 0.8, 1.0$ and 1.8, respectively. A common observation from these critical values is that for the lower values of β, the existence domain of the second solution shrinks. It is clear that both upper and lower branches of local Nusselt number depicts the decreasing trend for greater values of power-law parameter and these effect are more prominent in lower branch.

The nanoparticle concentration at the wall $\phi(0)$ is explained in **Fig**. **3.3** to visualize the influence of both the velocity-slip parameter and power-law parameter. Again, these plots delineate the critical range of shrinking parameter A for the existence of more than one solutions and this range is ended by critical value A_c. We can control the critical values by setting up different numerical values to the problem physical parameters. In addition, the plots given in both these figures display that a growth in power-law parameter β is to lessen the wall nanoparticle concentration for first solution and a reverse trend of the wall nanoparticle concentrations is seen in second solution. It may be noted through both figures that for a given A, the first solution has a greater value of $\phi(0)$ than the second solution. Moreover, it is worth mentioning that the existence range of dual solution shrinks in the absence of velocity-slip. **Table 3.1** shows the critical values of **Figs. 3.1** to **3.3.**

Fig. 3.4 indicates the effect of stretching/shrinking parameter A on temperature $\theta(\eta)$, it is clear that both solutions exist. First solution reduces, with the enlargement of stretching/shrinking parameter A, but the opposite trend can be seen in the second solution.

Figs. **3.5** to **3.7** indicate the effect of mass transfer parameter s on the skin friction $f''(0)$ and Nesselt number $\mathrm{Re}^{-1/2} Nu_x$, nanoparticles concentration at the wall $\phi(0)$ for different values of stretching/shrinking parameter A respectively. The critical point A_c decreases from -5.1888 to -5.6389 for increasing of mass transfer parameter. **Fig**. **3.5** indicates decreasing and increasing behaviour of the skin friction $f''(0)$ for the dual solution (first and second solutions respectively) for increasing suction parameter s. Similar trend can be noticed in **Fig. 3.6**. In **Fig**. **3.7,** the nanoparticles concentration at the wall $\phi(0)$ for increasing of suction parameter s gives an increasing behaviour in the upper branch solution and no solution exist for $A_c < A$.

From **Figs. 3.8** to **3.10**, the impacts of mass suction parameter s on the flow past the shrinking sheet for velocity, temperature and concentration profiles are pictured. It is seen through **Fig. 3.8** that, the dual nature of non-dimensional velocity is depicted for distinct

values of mass transfer parameter s. For first solution, we noticed that as the suction parameter is raised the velocity increases, besides profiles of velocity are depressed with higher s for second branch solution. On the other a quite opposite is true for momentum boundary layer thickness because it reduces for first solution and increases for second solution with a boost in suction. A substantial change is seen for higher value of s for second branch solution. For temperature $\theta(\eta)$ decreases in both solutions. From **Fig. 3.10,** it is concluded that in first solution, the nanoparticle volume friction $\phi(\eta)$ rises in a small region near the surface for increasing values of s but after a certain distance from the surface this profile start falling for a given value of η until the far field boundary condition is asymptotically satisfied. The reverse trend can be seen for the second solution.

Moreover, the effect of mass transfer parameter s on the skin friction $f''(0)$ for various values of Hartmann number Ha is discussed (see **Fig. 3.11**). It can be seen that no solution exists for $s < s_c$ and first solution is found higher.

The variation of velocity distribution $f'(\eta)$ (both first and second solutions) for distinct values of Hartmann number Ha are presented in **Fig. 3.12.** We notice in this figure that, the fluid velocity improves with growing values of Ha in case of the upper solution. Additionally, greater values of Hartmann number causes the thickness of momentum boundary layer to be depressed in this situation. But, for the second solution it decreases with Ha at fixed η. **Fig. 3.13** interprets the behaviour of dual temperature profiles for varying values of Hartmann number Ha by taking all other parameters fixed. Here, it is of worth mentioning that all plots approach the far field boundary conditions asymptotically. In accordance with the dual temperature profiles shown in this figure, it is sighted that the temperature is reduced in the first solution with increasing of Ha which is quite opposite to the case of second solution. Hence, for a particular set of physical parameters, the temperature of fluid for the second solution increases as Hartmann number Ha raises. The physical phenomenon of Lorentz force cause a slower movement of fluid, which corresponds to the reduction of the rate of heat transfer and hence the thermal boundary layer thickness decline by the greater Ha for first solution. However, in case of the second solution, thickness of thermal boundary layer is seen to be boosted up.

The influence of velocity slip parameter α on skin friction $f''(0)$ for various values of mass

transfer parameter s is displayed in **Fig. 3.14**. It can be noticed that the critical value A_c decreases from -0.5279 to -1.0138. and no solution exists for $s < s_c$.

The velocity, temperature and concentration profiles have been shown in **Figs. 3.15** to **3.17** satisfy the far field boundary conditions asymptotically, to gives the validation of numerical results and the existence of dual solutions. As we can view from **Fig. 3.15** that the fluid velocity has ascended trend with the enhancement in the velocity-slip parameter for the upper branch solution while a significant reduction in the boundary layer thickness is noted. Moreover, in case of lower solution the results are quite different. It is concluded that the dimensionless velocity reduces in a small region near the sheet for increasing values of α but after a certain distance from the sheet these profiles start growing for a given value of η until the far field boundary condition is asymptotically satisfied. As plotted in **Fig. 3.16** with an elevation in the velocity-slip parameter α, magnitude of the temperature drops off for both first and second solutions as well the thickness of thermal boundary layer. Further, it is noted that in case of first solution, the thermal boundary layer thickness is thinner as compared to the second solution. It can also be observed that rises in velocity slip parameter α, the concentration profile reduces in the first solution and rises in second solution (see **Fig. 3.17**).

Fig. 3.18 prescribes the variations of the non-dimensional temperature profile for numerous values of temperature ratio parameter θ_w for $A = -1.1$ (in the dual solution range). As should be obvious from this figure, thickness of the thermal boundary layer and non-dimensional temperature profile for the first solution is smaller than that of the second solution. It is interesting to see that both the solution exhibit a significant growth in fluid temperature by larger θ_w.

The influence of radiation parameter Nr on the temperature distribution $\theta(\eta)$ are imparted though **Fig. 3.19** for non-zero values of other physical parameters. It is found that in case of $A\,(= -1.1)$, there are two solutions for temperature profiles for various values of Nr. The upper branch of temperature profiles decreases with an up growing radiation parameter and also the thermal boundary layer thickness becomes thinner. However, when considering the second solution branches, the temperature profile increases with a rise in radiation parameter within the thermal boundary layer and converse is true away from the sheet, until it fulfill the far field condition. It is further depicted that, the temperature is high within the boundary

layer with small value of radiation parameter.

Moreover, the effect of nanofluid parameters (thermophoresis and Brownian motion parameters Nt and Nb respectively) on nanoparticle concentration has been displayed. The gradient of nanoparticle concentration at the surface is controlled passively by product of $\left(-\frac{Nt}{Nb}\right)$ and temperature gradient. So the nanoparticle concentration gradient rises with Nt and reduces with Nb. From **Fig. 3.20**, the concentration of nanoparticle $\phi(\eta)$ increases with Nt on both solutions, because of the way that the thermophoretic force takes away the fluid from the surface rapidly, which prompts to an increase in the concentration boundary layer thickness. Meanwhile, an inverse pattern can be watched for Nb and concentration boundary layer thickness reduces.

The impact of Nt on the temperature distribution has been discussed (see **Fig. 3.21**). Dual profiles depicts that in both solutions, strong influence in Nt leads to enhance the temperature of nanofluids. Moreover, the thermal boundary layer increases with higher Nt.

The variety of Nusselt number with Nr for different values of s and Nt in the absence ($Ec = 0$) and presence ($Ec = 0.05$) of viscous dissipation parameter Ec (which controls the fluid flow) is presented in **Figs. 3.22** to **3.23**. The dual solutions exist. From **Fig. 3.22**, the behaviour of Nusselt number increases for both solutions and first solution is always higher than the second solution. The ratio of convective and conductive heat transfer is named as Nusselt number, so for large Nusselt number, heat convection arises. Meanwhile the increasing value of Nt, the Nusselt number reduces for both solutions in the absence and presence of Eckert number Ec. Here it is also noticed that the first solution is higher than the second solution (see **Fig. 3.23**).

Table **3.1:** Critical values A_c for various values of β with $\alpha = 0$ and 0.1, other parameters are fixed.

β	α	A_c
0.8	0	-4.6426
1.0		-4.3859
1.8		-3.6311
0.8	0.1	-5.5340
1.0		-5.1880
1.8		-4.2019

Table 3.2: Calculated numbers of the skin friction $f''(0)$ for different A with $\beta = 1.0$ and $Ha = 0 = \alpha = s$.

A	Wang[34]	Yacob and Ishak[35]	Present results
5.0	-10.26475	–	-10.2647
3.0	–	–	-4.27654
2.0	-1.88731	-1.88731	-1.8873
1.0	0	0	0
0.5	0.7133	0.713295	0.71329
0.0	1.232588	1.232588	1.23259

Table 3.3: Calculated numbers of $f''(0)$ for upper and lower solution with different values of A by keeping $\beta = 1.0$, $Ha = 0 = \alpha = s$.

Upper solution () and lower solution []

	Wang[34]		Gorla et al.[36]		Present results	
A	()	[]	()	[]	()	[]
-0.25	1.40224	–	1.40225	–	1.40222	–
-0.50	1.4957	–	1.49566	–	1.49566	–
-0.75	1.48930	–	1.48928	–	1.48929	–
-1.00	1.32882	0	1.32881	0	1.32881	0
-1.15	1.08223	0.116702	1.08223	0.11670	1.08222	0.116702
-1.20	–	–	0.93247	0.23363	0.932472	0.23365
-1.2465	0.55430	–	–	–	0.584279	0.554296

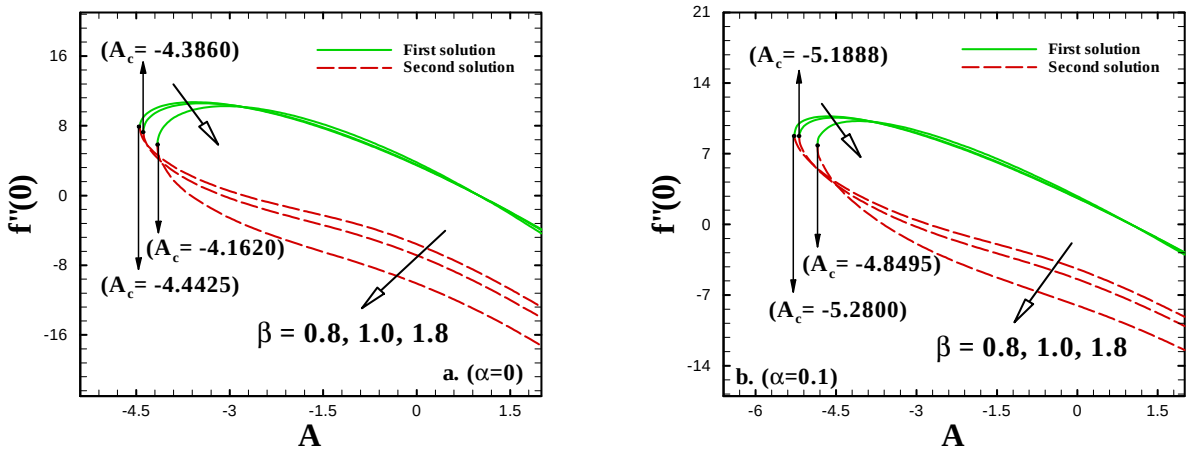

Fig. 3.1: Variation of skin friction $f''(0)$ with power law parameter β.

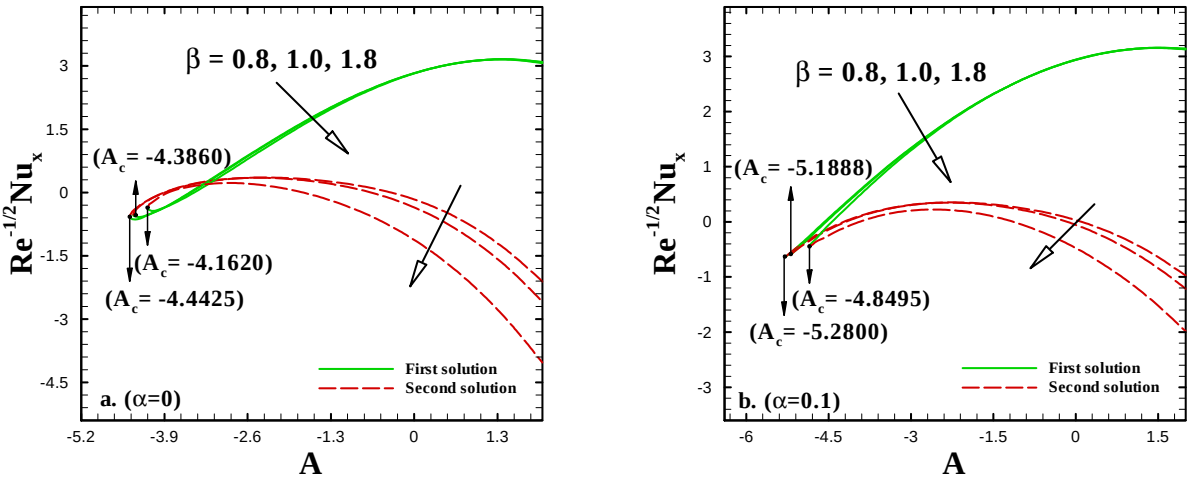

Fig. 3.2: Variation of Nusselt number $\mathrm{Re}^{-1/2}\, Nu_x$ with power law parameter β.

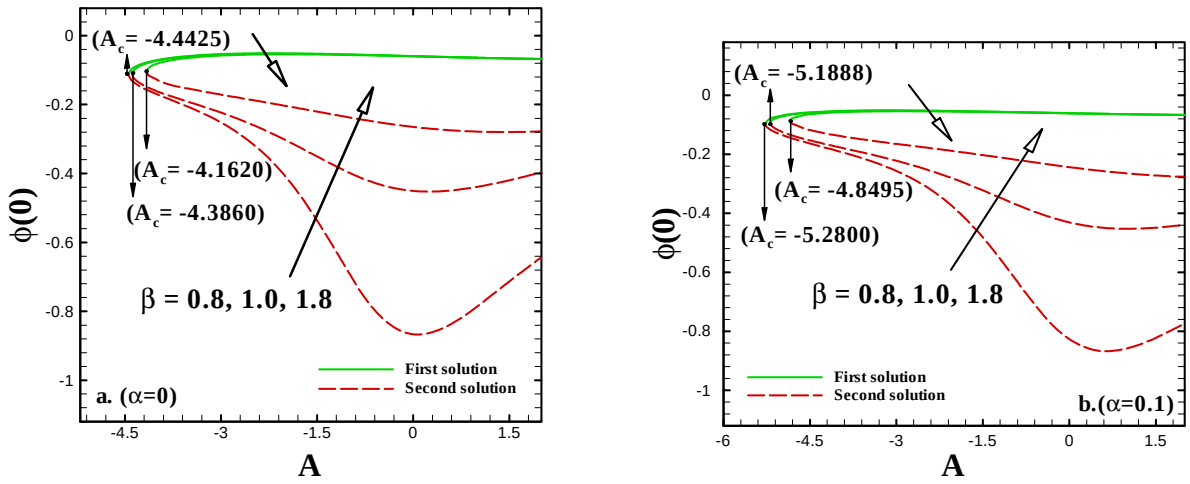

Fig. 3.3: Variation of nanoparticle concentration at the wall $\phi(0)$ with power law parameter β.

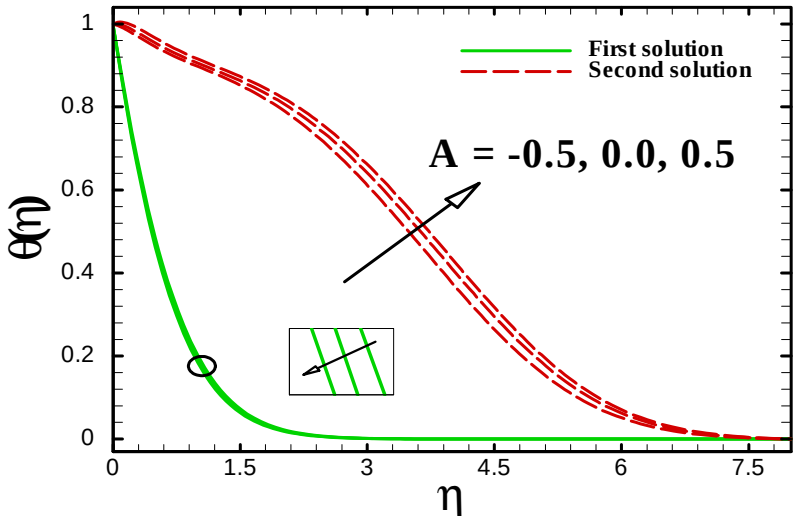

Fig. 3.4: The effect of stretching/shrinking parameter A on temperature profile $\theta(\eta)$.

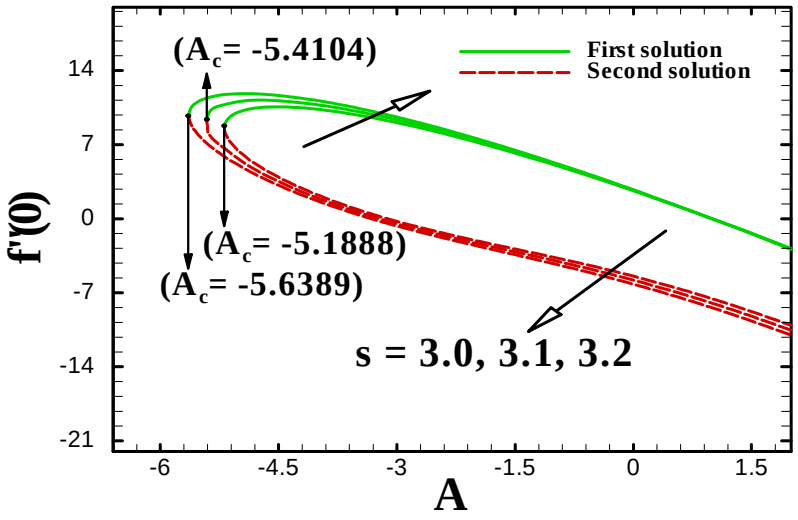

Fig. 3.5: The effect of stretching/shrinking parameter A on skin friction $f''(0)$.

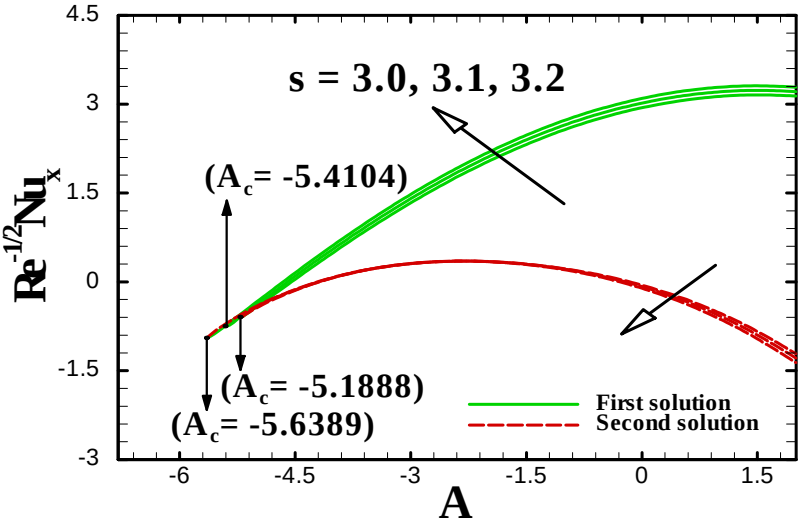

Fig. 3.6: The effect of suction parameter s on Nusselt number $\mathrm{Re}^{-1/2}\, Nu_x$ against A.

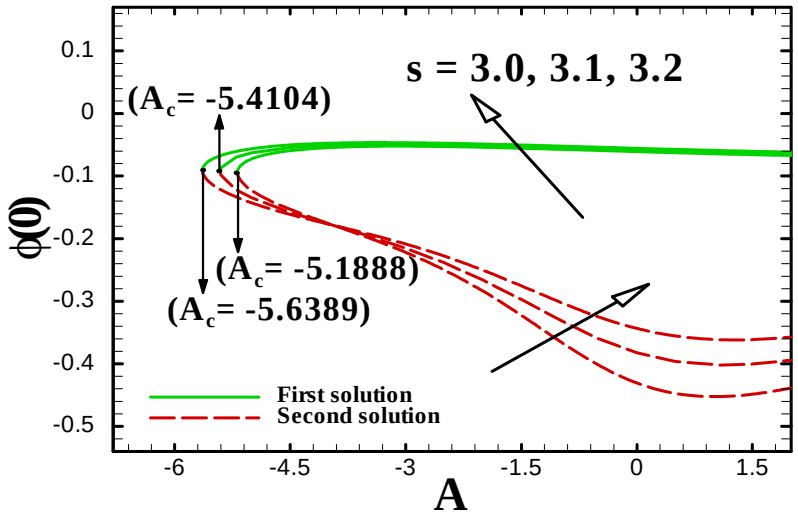

Fig. 3.7: The effect of suction parameter s on concentration of nanoparticle at the wall $\phi(0)$.

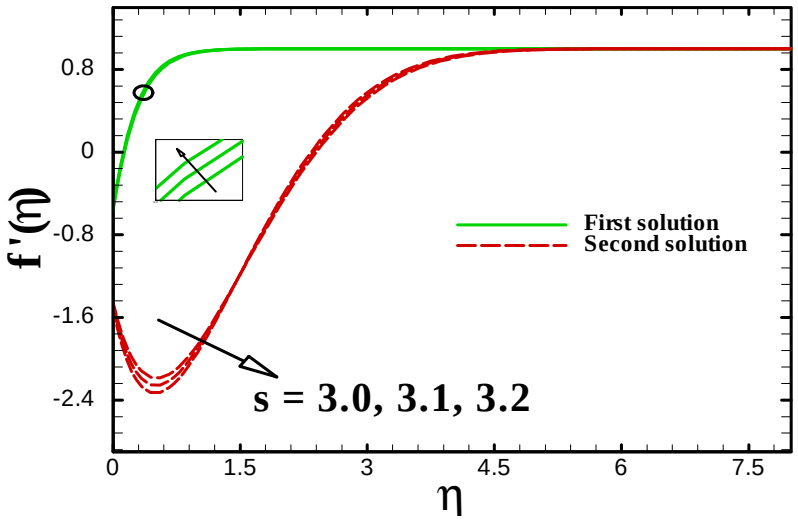

Fig. 3.8: The effect of suction parameter s on velocity profile $f'(\eta)$.

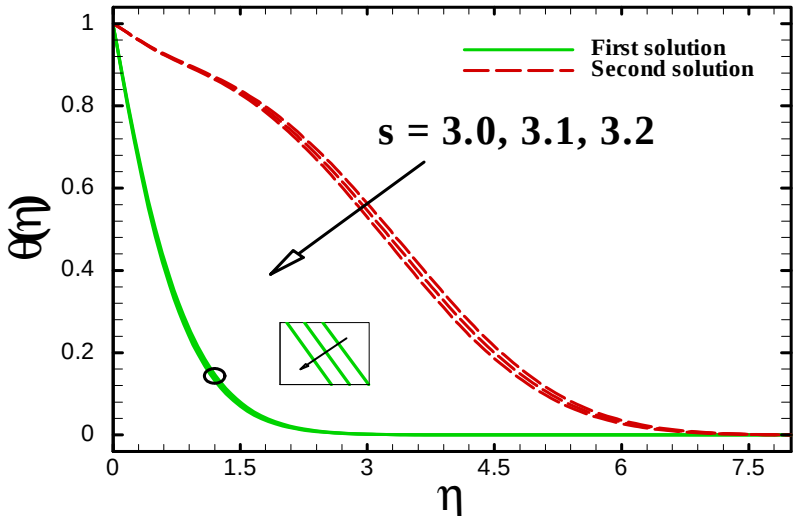

Fig. 3.9: Temperature profile $\theta(\eta)$ for various values of suction parameter s.

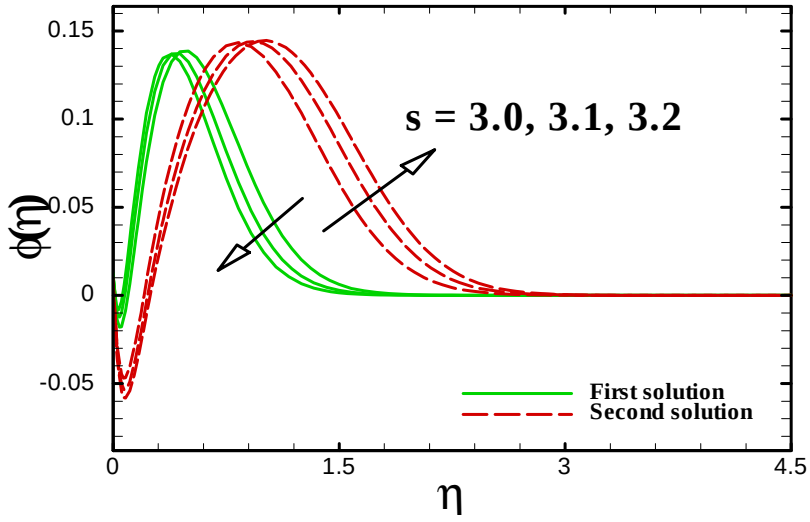

Fig. 3.10: concentration $\phi(\eta)$ profile for various values of suction parameter s.

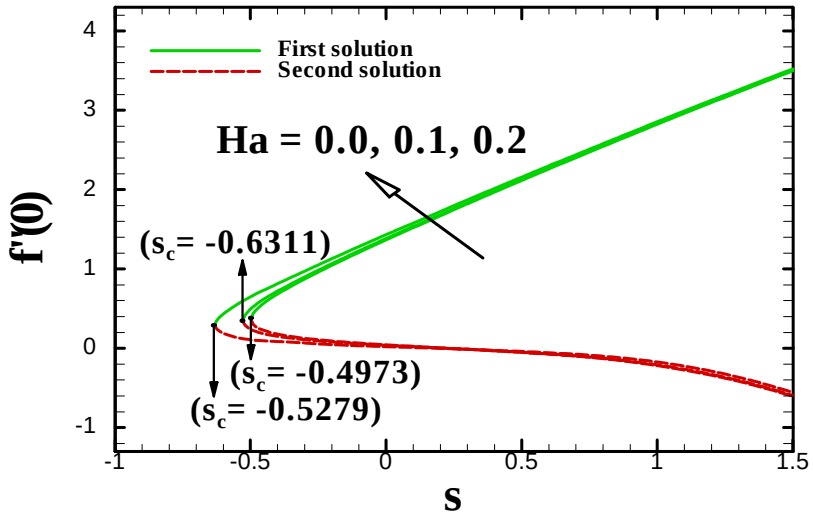

Fig. 3.11: Skin friction $f''(0)$ for various values of Hartmann number Ha.

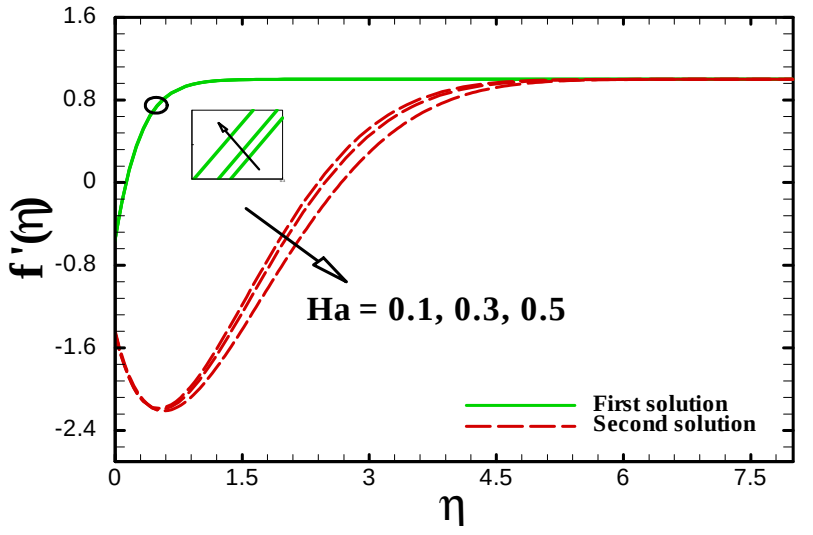

Fig. 3.12: Velocity profile $f'(\eta)$ for various values of Hartmann number Ha.

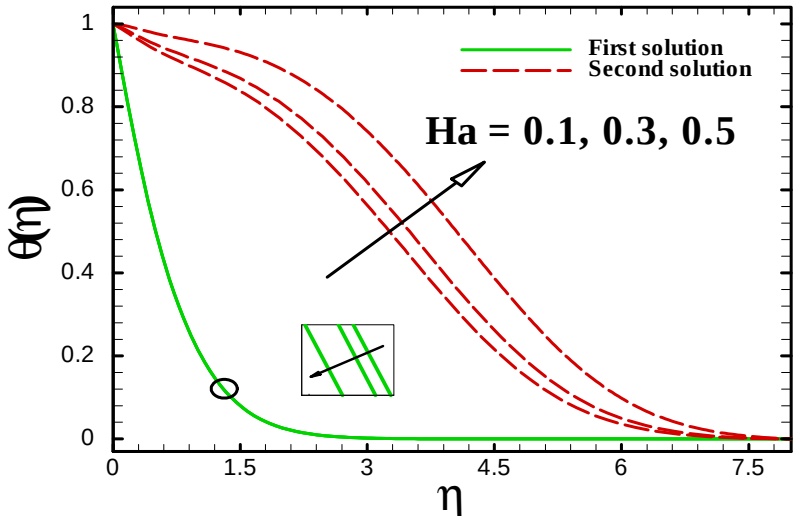

Fig. 3.13: Temperature profile $\theta(\eta)$ for different values of Hartmann number Ha.

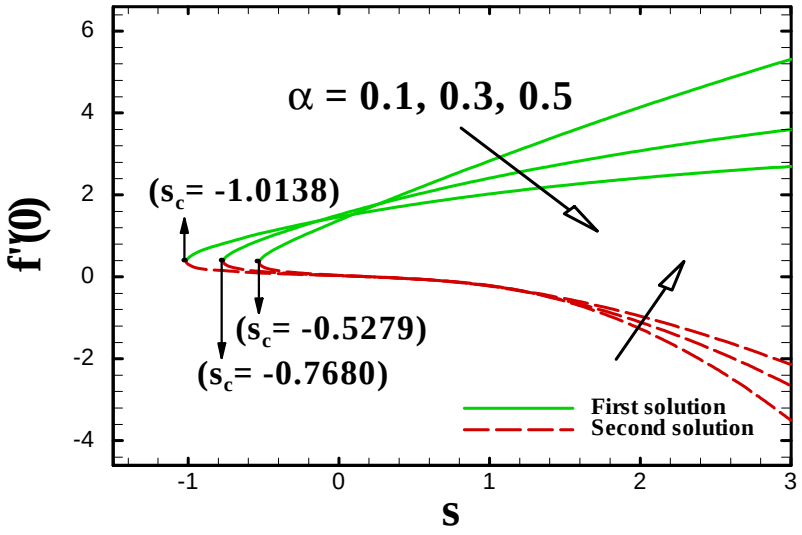

Fig. 3.14: The effect of slip parameter α on skin friction at the wall $f''(0)$.

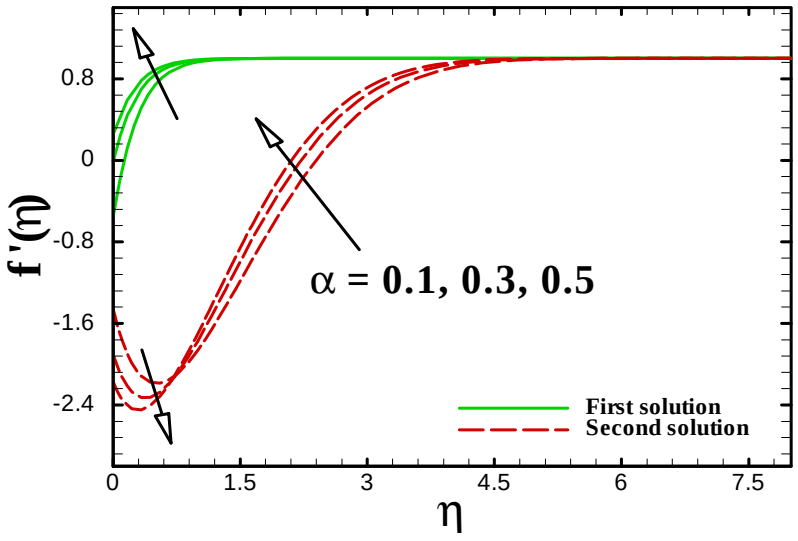

Fig. 3.15: Velocity profile $f'(\eta)$ for various values of velocity slip parameter α.

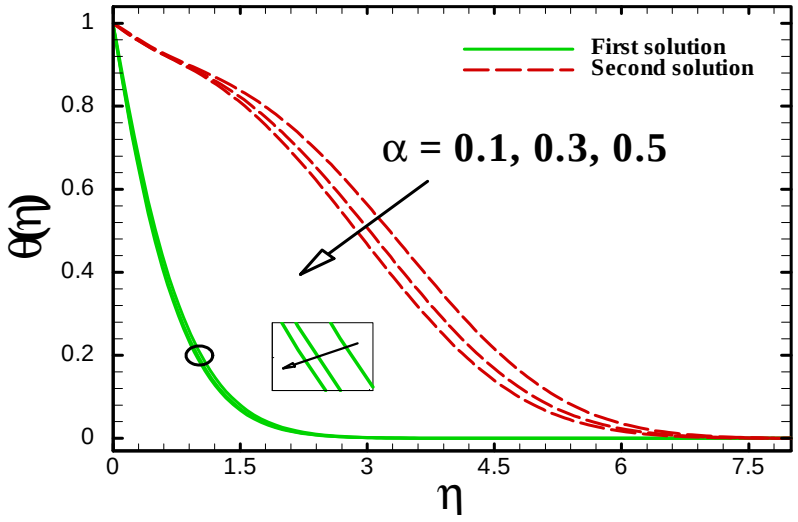

Fig. 3.16: Temperature profile $\theta(\eta)$ for various values α.

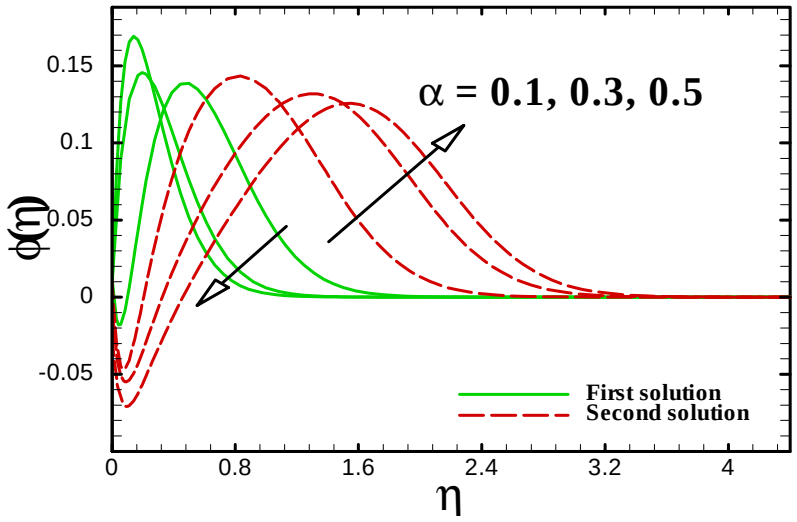

Fig. 3.17: Concentration profile $\phi(\eta)$ for various values of α when $Pr = 5, A = -5$.

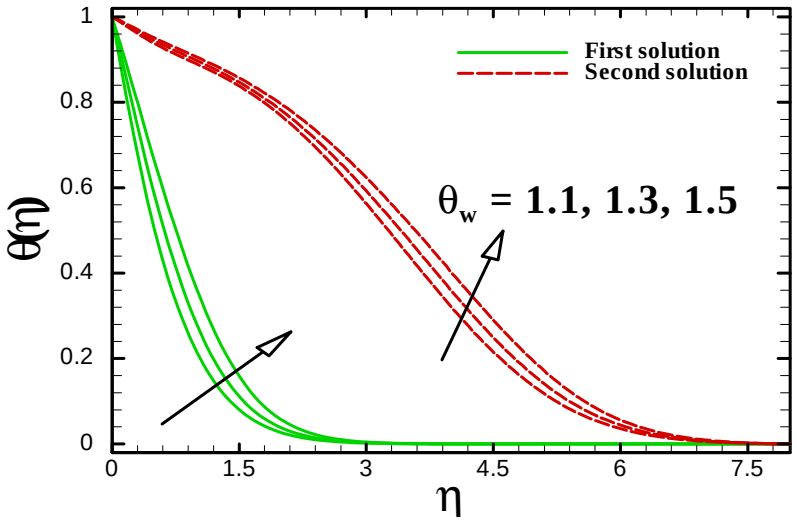

Fig. 3.18: The effect of temperature ratio parameter θ_w on temperature profile $\theta(\eta)$.

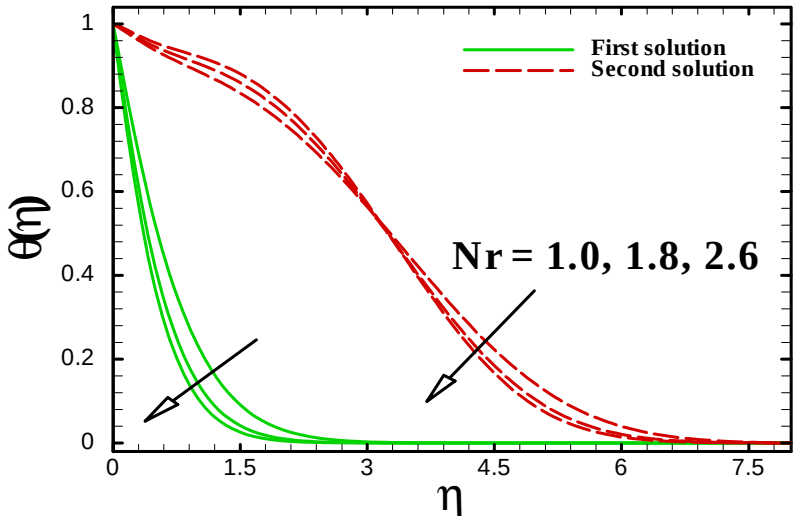

Fig. 3.19: The impact of radiation parameter Nr on temperature profile $\theta(\eta)$.

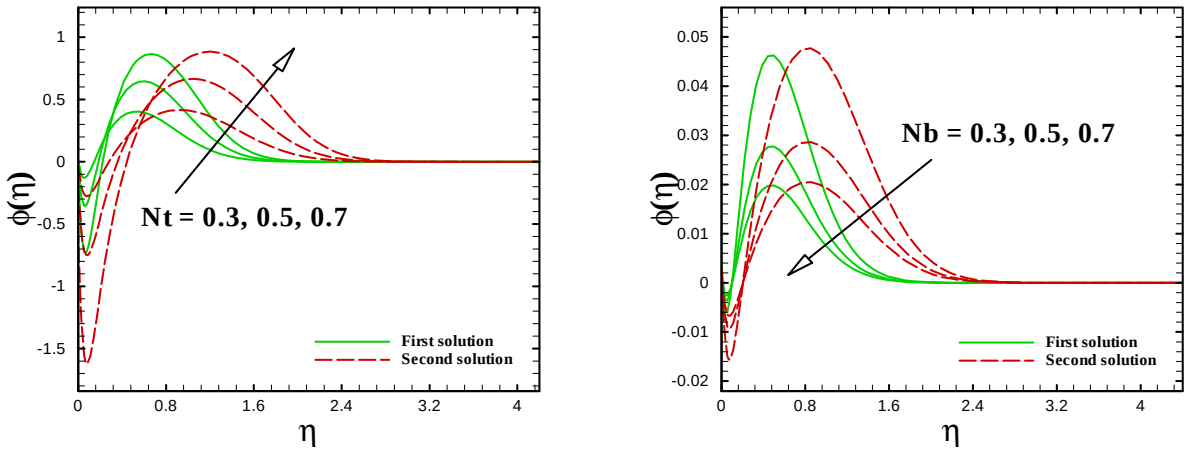

Fig. 3.20: Concentration profile $\phi(\eta)$ for various values of nanofluid parameters when $\Pr = 5$, $A = -5$.

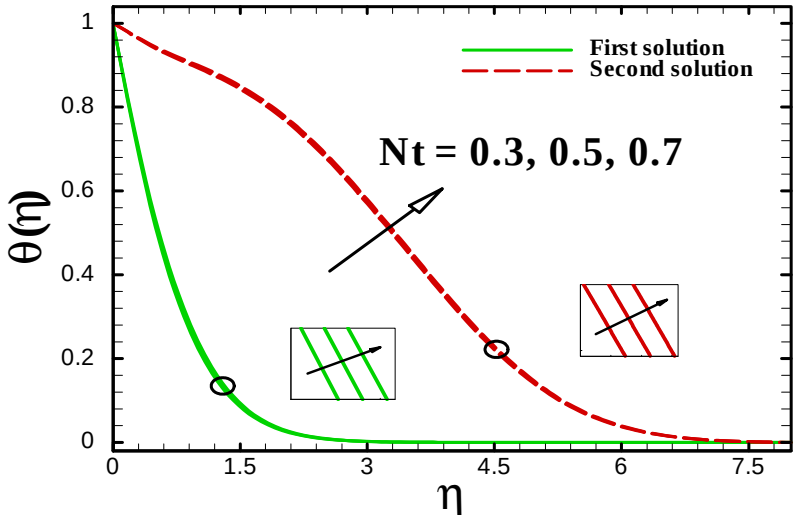

Fig. 3.21: Temperature profile $\theta(\eta)$ for different values of Nt.

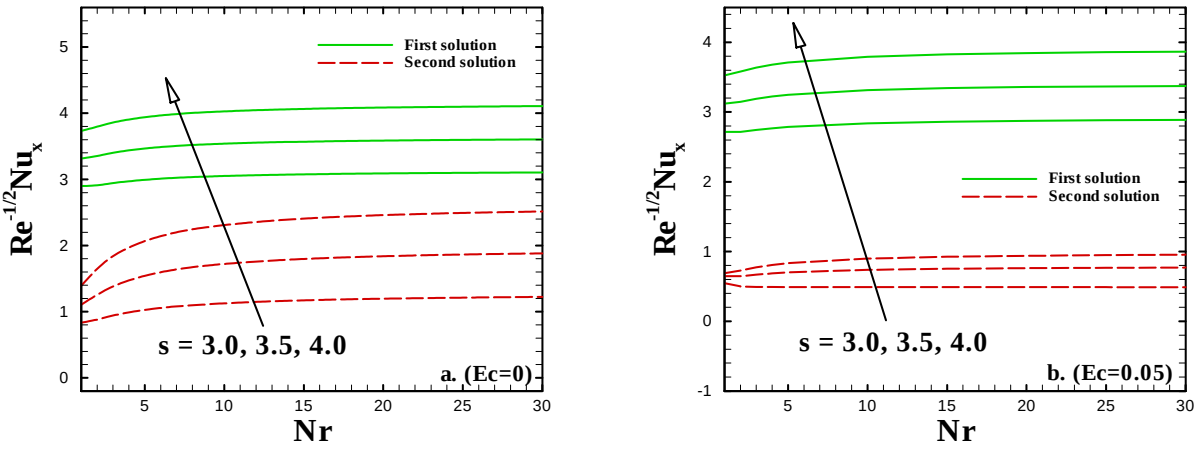

Fig. 3.22: The influence of radiation parameter Nr for Nusselt number $\mathrm{Re}^{-1/2}\, Nu_x$.

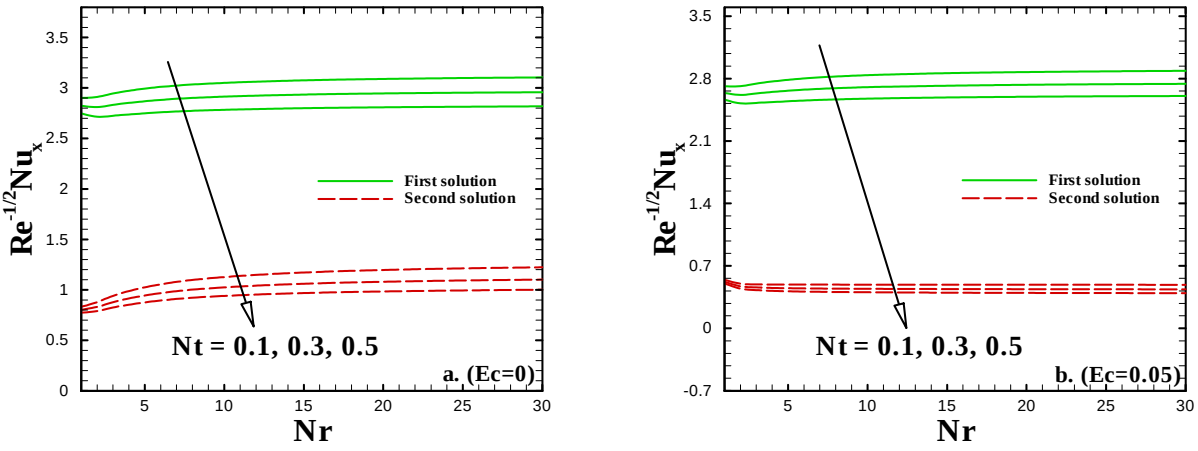

Fig. 3.23: The influence of thermophoresis parameter Nt for Nusselt number $\mathrm{Re}^{-1/2}\, Nu_x$.

3.4 Conclusions

This chapter presents a theoretical study for the existence of dual similarity solutions for flow on a moving plate in nanofluids. The effects of slip-flow in the vicinity of stagnation-point along with non-linear radiative heat transfer has been further investigated. For the computational intent, Matlab function bvp4c is utilized to achieve the dual solution. At last, there are few important results for this chapter obtained as:

- At the surface, the local skin friction and local Nusselt number are higher for lower power-law parameter in both solutions.
- The presence of velocity-slip widens the range of A for which dual solution exists.
- The mass suction parameter predicts the dominant effects for the skin friction.
- It is found that the nanoparticles concentration at the wall is raised by the suction parameter for first solution.
- As per subjective perspective, both temperature ratio parameter and radiation parameter have inverse impacts on the fluid temperature.

Bibliography

[1] U.S. Choi and J.A. Eastman, Enhancing thermal conductivity of fluids with nanoparticles, ASME Int. Mech. Eng. Congr. Exposition, San Francisco, (1995).

[2] J. Buongiorno, Convective transport in nanofluids, ASME J. Heat Transf., 128 (2006) 240 − 250.

[3] W. Khan and I. Pop, Boundary-layer flow of a nanofluid past a stretching sheet, Int. J. Heat Mass Transf., 53 (2010) 2477 − 2483.

[4] O.D. Makinde and A. Aziz, Boundary layer flow of a nanofluid past a stretching sheet with a convective boundary condition, Int. J. Therm. Sci., 50 (2011) 1326 − 1332.

[5] S. Nadeem and R.U. Haq, Effect of thermal radiation for megnetohydrodynamic boundary layer flow of a nanofluid past a stretching sheet with convective boundary conditions, J. Comp. Theor. Nanosci., 11 (2014) 32 − 40.

[6] T. Hayat, M.I. Khan, M. Waqas, T. Yasmeen and A. Alsaedi, Viscous dissipation effect in flow of magnetonanofluid with variable properties, J. Mol. Liq., 222 (2016) 47 − 54.

[7] Hashim and M. Khan, A revised model to analyze the heat and mass transfer mechanisms in the flow of Carreau nanofluids, Int. J. Heat Mass Transf., 103 (2016) 291 − 297.

[8] M. Khan, W.A. Khan and A.S. Alshomrani, Non-linear radiative flow of three-dimensional Burgers nanofluid with new mass flux effect, Int. J. Heat Mass Transf., 101 (2016) 570−576.

[9] N. Sandeep, Effect of aligned magnetic field on liquid thin film flow of magnetic-nanofluids embedded with graphene nanoparticles, Advanced Powder Tech., 28 (2017) 865 − 875.

[10] T. Hayat, M.I. Khan, M. Waqas, A. Alsaedi and M. Farooq, Numerical simulation for melting heat transfer and radiation effects in stagnation point flow of carbon–water nanofluid, Comput. Meth. Appl. Mech. Eng., 315 (2017) 1011 – 1024.

[11] C.S.K. Raju and N. Sandeep, Unsteady Casson nanofluid flow over a rotating cone in a rotating frame filled with ferrous nanoparticles: A numerical study, J. Mag. Mag. Mat., 421 (2017) 216 – 224.

[12] P. Besthapua, R.U. Haq, S. Bandaria and Q.M. Al-Mdallalc, Mixed convection flow of thermally stratified MHD nanofluid over an exponentially stretching surface with viscous dissipation effect, J. Taiwan Inst. Chem. Eng., 71 (2017) 307 – 314.

[13] A.Y. Bakier, Thermal radiation effect on mixed convection from vertical surface in saturated porous media, Int. Commun. Heat Mass Transf., 28 (1) (2001) 119 – 126.

[14] R. Cortell, Effects of viscous dissipation and radiation on the thermal boundary layer over a non-linearly stretching sheet, Phys. Lett. A, 372 (2008) 631 – 636.

[15] N.S. Akber, S. Nadeem, R. Ul Haq and Z.H. Khan, Radiation effects on MHD stagnation point flow of nanofluid towards a stretching surface with convective boundary condition, Chin. J. Aeronaut., 26 (6) (2013) 1389 – 1397.

[16] M. Sheikholeslami, D.D. Ganji, M.Y. Javed and R. Ellahi, Effect of thermal radiation on magnetohydrodynamics nanofluid flow and heat transfer by means of two phase model, J. Magn. Magn. Mater., 374 (2015) 36 – 43.

[17] M. Khan, Hashim, M. Hussain and M. Azam, Magnetohydrodynamic flow of Carreau fluid over a convectively heated surface in the presence of non-linear radiation, J. Magn. Magn. Mater., 412 (2016) 63 – 68.

[18] C.L.M. Navier, Sur les lois du mouvement des fluids, C.R. Acad. Sci. France, 6 (1827) 389 – 440.

[19] F. Sharipov and V. Seleznev, Data on internal rarefied gas flows, J. Physi. Chem. Ref. Data, 27 (1998) 657 – 706.

[20] C.Y. Wang, Flow over a surface with parallel grooves, Phys. Fluids, 15 (2003) $1114-1121$.

[21] C.H. Choi and C.J. Kim, Large slip of aqueous liquid flow over a nanoengineered superhydrophobic surface, Phys. Rev. Lett., 96 (2006) 066001.

[22] C.Y. Wang, Flow due to a stretching boundary with partial slip-an exact solutions of the Navier–Stokes equations, Chem. Eng. Sci., 57 (2002) $3745-3747$.

[23] T. Hayat, T. Javed and Z. Abbas, Slip flow and heat transfer of a second grade fluid past a stretching sheet through a porous space, Int. J. Heat Mass Transf., 51 (2008) $4528-4534$.

[24] S. Mukhopadhyay, Analysis of boundary layer flow over a porous nonlinearly stretching sheet with partial slip at the boundary, Alexandria Eng. J., 52 (2013) $563-569$.

[25] S. Nadeem, R. Mehmood, N.S. Akbar, Combined effects of magnetic field and partial slip on obliquely striking rheological fluid over a stretching surface, J. Magn. Magn. Mater., 378 (2015) $457-462$.

[26] M. Khan and Hashim, Effects of multiple slip on flow of magneto-Carreau fluid along wedge with chemically reactive species, Neural Comput & Applic., (2016).$doi : 10.1007/s00521-016-2825-3$.

[27] R. Dhanai, P. Rana, and L. Kumar, Multiple solutions of MHD boundary layer flow and heat transfer behavior of nanofluids induced by a power-law stretching/shrinking permeable sheet with viscous dissipation, P. Tech., 273 (2015) $62-70$.

[28] R. Cortell, Viscous flow and heat transfer over a nonlinearly stretching sheet, Appl. Math. Comput., 184 (2) (2007) $864-873$.

[29] T. Javed, Z. Abbas, M. Sajid and N. Ali, Heat transfer analysis for a hydromagnetic viscous fluid over a non-linear shrinking sheet, Int. J. Heat Mass Transf., 54 (9) (2011) $2034-2042$.

[30] Z. Abbas, and T. Hayat, Radiation effects on MHD flow in a porous space, Int. J. Heat Mass Transf., 51 (5) (2008) $1024-1033$.

[31] T. Fang and J. Zhang, Closed-form exact solutions of MHD viscous flow over a shrinking sheet, Communi. Nonlinear Sci. Numerical Simulation, 14 (7) (2009) $2853-2857$.

[32] S. Rosseland, Astrophysik und Atom-Theoretische Grundlagen, SpringerVer-lag, Berlin, (1931) 41 – 44.

[33] A.V. Kuznetsov and D.A. Nield, Natural convection boundary-layer of a nanofluid past a vertical plate: a revised model, Int. J. Therm. Sci., 77 (2014) 126 – 129.

[34] C.Y. Wang, Stagnation flow towards a shrinking sheet, Int. J. Nonlinear Mech., 43 (2008) 377 – 382.

[35] N.A. Yacob and A. Ishak, Stagnation point flow towards a stretching/shrinking sheet in a micropolar fluid with a convective surface boundary condition, Can. J. Chem. Eng., 90 (2012) 621 – 626.

[36] R.S.R. Gorla and B.J. Gireesha, Dual solutions for stagnation-point flow and convective heat transfer of a Williamson nanofluid past a stretching/shrinking sheet, Heat Mass Transf., 52 (2016) 1153 – 1162.